J. Fluid Mech. (1980), *vol.* 98, *part* 2, *pp.* 349–381
Printed in Great Britain

The radiation of sound by the instability waves of a compressible plane turbulent shear layer

By CHRISTOPHER K. W. TAM
Department of Mathematics, Florida State University, Tallahassee, Florida 32306

AND PHILIP J. MORRIS
Department of Aerospace Engineering, The Pennsylvania State University, University Park, Pennsylvania 16802

(Received 8 July 1977 and in revised form 2 October 1979)

The problem of acoustic radiation generated by instability waves of a compressible plane turbulent shear layer is solved. The solution provided is valid up to the acoustic far-field region. It represents a significant improvement over the solution obtained by classical hydrodynamic-stability theory which is essentially a local solution with the acoustic radiation suppressed. The basic instability-wave solution which is valid in the shear layer and the near-field region is constructed in terms of an asymptotic expansion using the method of multiple scales. This solution accounts for the effects of the slightly divergent mean flow. It is shown that the multiple-scales asymptotic expansion is not uniformly valid far from the shear layer. Continuation of this solution into the entire upper half-plane is described. The extended solution enables the near- and far-field pressure fluctuations associated with the instability wave to be determined. Numerical results show that the directivity pattern of acoustic radiation into the stationary medium peaks at 20 degrees to the axis of the shear layer in the downstream direction for supersonic flows. This agrees qualitatively with the observed noise-directivity patterns of supersonic jets.

1. Introduction

This paper considers the radiation of sound associated with an artificially-excited spatially-growing instability wave of a fixed frequency, in a plane turbulent shear layer. This work is an outgrowth of the authors' effort to understand the mechanisms of jet-noise generation. During the past few years a number of investigators, e.g. Sedel'nikov (1967), Tam (1971, 1972, 1975), Bishop, Ffowcs Williams & Smith (1971), Morris (1974) and Liu (1974) suggested that flow instabilities could play a very important role in supersonic jet-noise generation. This idea was confirmed in a series of experiments by McLaughlin, Morrison & Troutt (1975, 1977) using supersonic jets with low to moderately-high Reynolds numbers. To facilitate experimental measurements of the relative phase of the instability waves at different locations in the jet, the jet was gently excited by glow discharge at the nozzle exit at certain selected frequencies. Hot-wire and microphone measurements indicated the presence of spatially-growing flow instability waves together with strong noise radiation at the forced frequencies. The experimental situation just described is quite similar to the

0022–1120/80/4448–1010 $02.00

model problem under consideration in this paper. For cold subsonic jets no direct experimental evidence is available at this time to show whether the same mechanism is important in producing noise. For a heated subsonic jet with exit Mach number 0·7 and exit temperature 900 K, Dahan & Élias (1976) determined that noise was radiated from large-scale motions of the jet which had the local characteristics of wavelike instabilities of the jet. Chan (1974*a*, *b*; 1976) and Moore (1977) have demonstrated that it is possible to excite instability waves in the shear layer of a turbulent subsonic jet. Further, when the amplitudes of the excited waves were small, they found that most of their characteristics agreed quite well with the predictions of classical linear inviscid hydrodynamic-instability theory. In recent years a number of workers have examined the jet flow or free shear-layer instability problem. Some of the more recent works, such as those by Morris (1974, 1976*a*, 1977), Liu (1974), Tam (1975), Chan (1975), Merkine & Liu (1975), and others emphasized the slight nonlinear aspects of the problem. On the other hand, a number of papers such as those by Bouthier (1972, 1973), Gaster (1974), Saric & Nayfeh (1975) and Crighton & Gaster (1976) discuss the modification to classical instability theory due to slight flow divergence which is inevitable in unbounded shear flows. In all these works, with the exception of Tam (1975) and Morris (1976*a*), no attempt was made to calculate the sound waves generated by the flow instabilities. Tam (1975) used physical reasoning to model the noise generation processes for supersonic jets and estimated the noise emitted. Unlike most of the works cited above, the sound radiation problem is the main question to be addressed here. In this paper the instability wave solution, which is valid in the shear layer and a near-field region, is constructed in terms of an asymptotic expansion using the method of multiple scales. This solution accounts for the effects of the slightly divergent mean flow. The instability-wave amplitude is assumed to be small so that nonlinear effects are ignored. In fact, even if its amplitude is not small, the nonlinear effects are only important inside the shear layer. In this case the present method still applies if the instability wave solution in the shear layer is appropriately modified. Classical hydrodynamic instability theory (see Lees & Lin 1946; Lin 1953; Gropengieser 1969; Blumen 1970, 1971) of a compressible plane mixing layer does not predict acoustic radiation. A closer examination of this solution (see § 2.3) reveals that it is a local solution and is valid only up to a limited region outside the shear layer. The solution presented in this paper, however, has uniform validity up to the acoustic far-field region.

In classical hydrodynamic instability theory of compressible flows such as boundary layers or free-shear layers, the parallel-flow approximation is invariably used. Because of this, the instability wave solution so obtained is valid only over a localized region. To determine the sound radiation associated with an instability wave, a global solution of the total wave propagation phenomenon is necessary. In a two-dimensional shear layer, because of entrainment, the mean flow diverges in the downstream direction. As a result the instability characteristics of the shear layer vary continuously from point to point in the streamwise direction. When an instability wave is initiated at a certain location of the flow by periodic external excitation, it will first undergo a rapid spatial growth. As the shear layer thickens, the growth rate decreases until finally the wave will reach a region where the shear layer is too thick to support an unstable wave at the forced frequency. Downstream of this region the wave will be damped. Its amplitude decreases as it continues to propagate until it is vanishingly small

Except in the case of very-high-speed flow, the phase velocity of the instability wave is usually subsonic relative to the stationary ambient gas. A subsonic wave with constant amplitude generates no sound. However, if the wave amplitude grows and decays spatially then some wave components would actually be moving with supersonic phase velocity which, as is well known, would lead immediately to acoustic radiation. Thus for the problem under consideration, the classical instability theory must be modified to allow for the phenomenon of mean-flow divergence and provide a description of the growth and decay of the excited instability wave.

Following the above reasoning a solution is first found for the instability wave in the shear layer. This solution is constructed using the method of multiple scales. The procedure adopted is very similar to the method of Saric & Nayfeh (1975). Here necessary modifications to deal with the singular behaviour of the damped inviscid eigenfunctions by contour deformation in the complex plane are made. (The damped inviscid eigensolutions are discussed in appendix B and are shown in §4.2 to be a valid approximation to the damped viscous solutions at high Reynolds number.) A fast and a slow spatial variable are introduced in the analysis. The slow variable is used to take into account the gradual divergence of the mean flow. The fast variable is the same one as used in the hydrodynamic instability theory. The higher-order terms in the multiple-scales expansion are obtained using the method of variation of parameters. Examination of these terms reveals that the multiple-scales asymptotic expansion is not uniformly valid far from the shear layer. It is thus argued that the present perturbation problem is singular. An extended solution which is a uniformly-valid asymptotic expansion for large distances from the shear layer is constructed by showing that a model boundary-value problem, for which a uniformly-valid expansion exists, is the continuation of the instability wave solution. The solution of this problem which provides the pressure fluctuations associated with the instability wave in the far field, is obtained by the method of Fourier transforms. The noise radiation is then readily calculated.

Before proceeding with the analysis and calculations it is felt to be useful, in view of the many separate steps that constitute the analysis, to provide a description of the mathematical strategy to be followed in the following sections. Section 2 develops the instability wave solution using the method of multiple scales. The solution of the eigenvalue problem, formed by the equation for the zeroth-order terms in the multiple-scales expansion and their boundary conditions, is provided in § 2.1. This enables the pressure fluctuation to be defined completely to order unity. Higher-order terms in the multiple-scales expansion are derived in §2.2 using the method of variation of parameters. The analytical form of these higher-order terms may be obtained in the uniform mean-flow region outside the shear layer. This analysis, given in § 2.3, shows that the multiple-scales asymptotic expansion is not uniformly valid at large distances from the edge of the shear layer. In § 3 a method is described which enables the solution for the instability wave to be continued into the region outside the shear layer. The necessary properties of this solution, referred to as the extended solution, are developed first. This extended solution is shown to be identical to a selected boundary-value problem in § 3.1. This identity is achieved by matching the boundary-value problem's boundary condition to the properties of the instability wave solution in a region close to the edge of the mixing layer. A uniformly-valid asymptotic expansion for the extended problem is obtained in § 3.2 using the method of Fourier transforms.

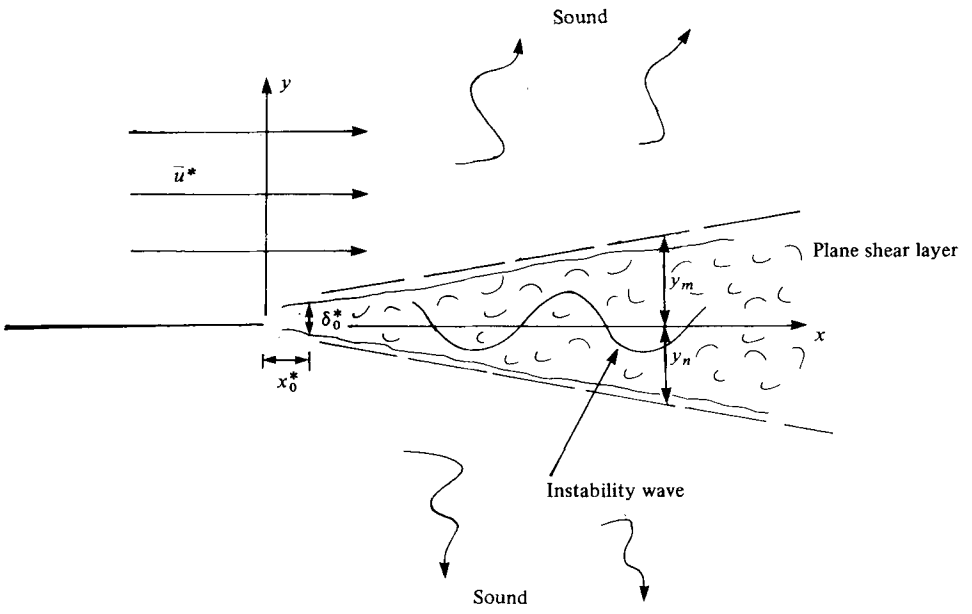

FIGURE 1. Plane shear-layer flow.

This enables the sound radiation associated with the instability wave to be calculated. The far-field solution associated with the multiple-scales asymptotic solution for the instability wave is evaluated in § 3.3 using the method of stationary phase.

In § 4 of this paper the method outlined above is applied to the acoustic radiation problem associated with an instability wave in a plane turbulent shear layer. Experimental measurements show that the mean velocity profile of the flow can be approximated by a complementary error function. Numerical results for the inviscid instability characteristics of the shear layer including local growth rate and wavenumber with or without divergent flow corrections are presented at several Mach numbers. Directivity patterns of acoustic radiation at subsonic and supersonic flow Mach numbers are also presented in this section. Because of flow similarity (there is a lack of intrinsic length and time scales in this free shear-layer problem) the directivity pattern is not sensitive to the frequency of the wave except in the extremely-high-frequency range. For supersonic flows the noise radiation peaks around 20 degrees to the axis of the shear layer in the ambient medium. This is qualitatively consistent with the experimental observations of Dosanjh & Yu (1968) for a turbulent supersonic jet. Further discussion of the numerical results in relation to jet noise radiation will be given at the end of this paper.

2. The multiple-scales instability-wave solution

The behaviour of small wave-like disturbances propagating in a pre-existing plane turbulent shear layer will be considered. These disturbances are assumed to be induced by a localized external periodic excitation of frequency ω^*. The basic flow is sketched in figure 1. The turbulent mixing layer has a small initial thickness, δ_0^* at $x^* = x_0^*$ which takes account of the boundary layer on the splitter plate. The mixing

layer has a constant rate of spread which will be assumed to be a known function of the free-stream Mach number, M. The static pressure and temperature will be assumed constant throughout the flow. This condition, which is physically realistic for an appropriately-heated uniform stream up to Mach numbers of close to two, may easily be relaxed. Since the mean velocity profile has characteristics which lead to dynamic instabilities of small perturbations, even in the absence of viscosity, the wavelike disturbances will be assumed to satisfy the linearized, inviscid, compressible equations of motion. To describe properly the behaviour of the excited periodic disturbances in the shear layer, it is important to take account of the divergence of the mean flow. Since the spreading rate of the mixing layer is small, especially at high free-stream Mach numbers, the method of multiple scales will be used to describe the disturbance behaviour. The governing equations are the linearized continuity, momentum and energy equations together with the equation of state.

All the physical variables are non-dimensionalized with respect to the corresponding free-stream quantities, such as the free-stream velocity $\bar{u}^*$, density $\bar{\rho}^*$, pressure $\bar{p}^*$, and the initial thickness of the mixing layer δ_0^*. The appropriate time scale is $\delta_0^*/\bar{u}^*$. The governing linearized equations of motion can readily be reduced to

$$\frac{\partial p'}{\partial t} + \bar{u}_j \frac{\partial p'}{\partial x_j} + \gamma \frac{\partial u_j'}{\partial x_j} = 0, \tag{2.1}$$

and

$$\gamma M^2 \left[\frac{\partial u_i'}{\partial t} + \bar{u}_j \frac{\partial u_i'}{\partial x_j} + u_j' \frac{\partial \bar{u}_i}{\partial x_j} \right] = -\frac{\partial p'}{\partial x_i}, \tag{2.2}$$

where primes denote fluctuating quantities and γ is the ratio of specific heats. The two-dimensional turbulent mean flow is a function of the transverse co-ordinate y, and a slowly varying function of axial distance x. Measured mean flow profiles will be used. From the measurements of Liepmann & Laufer (1947) the mean velocity vector may be written as

$$\bar{\mathbf{u}} = [U(y/s), \quad \epsilon V(y/s), 0], \tag{2.3a}$$

where

$$\left.\begin{aligned} U &= 0 \quad \text{for} \quad y \leqslant -y_n, \\ U &= 1 \\ V &= 0 \end{aligned}\right\} \quad \text{for} \quad y \geqslant y_m. \tag{2.3b}$$

In equations (2.3a, b) $s = \epsilon x$, where the small parameter ϵ is a measure of the rate of spread of the shear layer. Typically ϵ is less than 0·1. The mean velocity in the x direction is effectively zero below the mixing layer and the flow is uniform for $y \geqslant y_m$ as shown in figure 1. A solution will be sought to equations (2.1) and (2.2) in the form of a slowly-varying wave

$$p'(x, y, t) = \left\{ \sum_{n=0}^{\infty} \epsilon^n \hat{p}_n(y, s) \right\} e^{i\theta(x) - i\omega t}, \tag{2.4a}$$

$$u'(x, y, t) = \left\{ \sum_{n=0}^{\infty} \epsilon^n \hat{u}_n(y, s) \right\} e^{i\theta(x) - i\omega t} \tag{2.4b}$$

and

$$v'(x, y, t) = \left\{ \sum_{n=0}^{\infty} \epsilon^n \hat{v}_n(y, s) \right\} e^{i\theta(x) - i\omega t}, \tag{2.4c}$$

where ω is the forced frequency of the wave and the fast phase function, θ, is such that

$$d\theta/dx = \alpha(s). \tag{2.5}$$

This form of multiple-scales asymptotic expansion has been used previously by Saric & Nayfeh (1975) in their investigation of the non-parallel stability of boundary-layer flows. Substitution of (2.4) into (2.1) and (2.2) and ordering the equations in powers of ϵ gives, to order unity,

$$-i\hat{\omega}\hat{p}_0+\gamma(i\alpha\hat{u}_0+\partial\hat{v}_0/\partial y)=0, \tag{2.6a}$$

$$\gamma M^2\{\hat{v}_0\,\partial U/\partial y-i\hat{\omega}\hat{u}_0\}=-i\alpha\hat{p}_0, \tag{2.6b}$$

and

$$i\gamma M^2\hat{\omega}\hat{v}_0=\partial\hat{p}_0/\partial y, \tag{2.6c}$$

where

$$\hat{\omega}=\omega-\alpha U.$$

These equations readily reduce to a single equation for $\hat{p}_0$ of the form

$$\frac{\partial^2\hat{p}_0}{\partial y^2}+\frac{2\alpha}{\hat{\omega}}\frac{\partial U}{\partial y}\frac{\partial\hat{p}_0}{\partial y}-[\alpha^2-M^2\hat{\omega}^2]\hat{p}_0=0 \tag{2.7a}$$

which will be written as

$$L_y[\hat{p}_0]=0. \tag{2.7b}$$

To order ϵ a set of inhomogeneous equations for the fluctuations $\hat{p}_1$, $\hat{u}_1$ and $\hat{v}_1$ are obtained where the right-hand sides are functions of the zeroth-order fluctuations. These equations may be reduced to a single inhomogeneous equation for $\hat{p}_1$ of the form

$$\begin{aligned}L_y[\hat{p}_1]=&-2i(M^2U\hat{\omega}+\alpha)\frac{\partial\hat{p}_0}{\partial s}+\frac{2i\omega}{\hat{\omega}^2}\frac{\partial U}{\partial y}\frac{\partial^2\hat{p}_0}{\partial y\,\partial s}+i\left\{M^2U^2\hat{p}_0-\hat{p}_0+\frac{2\omega U}{\hat{\omega}^3}\frac{\partial U}{\partial y}\frac{\partial\hat{p}_0}{\partial y}\right\}\frac{d\alpha}{ds}\\&+i\left\{\frac{2\alpha^3V}{\hat{\omega}^2}\frac{\partial U}{\partial y}+\frac{4\alpha^2}{\hat{\omega}}\frac{\partial V}{\partial y}-\alpha M^2\left[U\frac{\partial V}{\partial y}+V\frac{\partial U}{\partial y}\right]-2M^2\hat{\omega}\frac{\partial V}{\partial y}\right\}\hat{p}_0\\&-i\left\{2M^2V\hat{\omega}-\frac{2\alpha(\hat{\omega}+\omega)}{\hat{\omega}^3}\frac{\partial U}{\partial y}\frac{\partial V}{\partial y}-\frac{2\alpha^2V}{\hat{\omega}^3}\left(\frac{\partial U}{\partial y}\right)^2\right\}\frac{\partial\hat{p}_0}{\partial y}\equiv\chi_1.\end{aligned} \tag{2.8}$$

Similarly the higher-order equations lead to inhomogeneous equations for $\hat{p}_n$ of the form

$$L_y[\hat{p}_n]=\chi_n(y,s),\quad n=1,2,3,\ldots. \tag{2.9}$$

The inhomogeneous term χ_n contains fluctuation quantities of lower order. For $y\geqslant y_m$ the mean flow is uniform and χ_n takes a simple form. In this region of uniform flow the value of χ_n will be denoted by $\bar{\chi}_n$ which is given by

$$\bar{\chi}_n(\hat{p}_{n-1},\hat{p}_{n-2})=-2i[M^2(\omega-\alpha)+\alpha]\frac{\partial\hat{p}_{n-1}}{\partial s}-i(1-M^2)\frac{d\alpha}{ds}\hat{p}_{n-1}-(1-M^2)\frac{\partial^2\hat{p}_{n-2}}{\partial s^2}. \tag{2.10}$$

(Note that in equation (2.10) $\hat{p}_{-2}=\hat{p}_{-1}=0$ and $\bar{\chi}_0=0$.)

2.1. *The eigenvalue problem*

The amplitude and phase functions of the multiple-scales asymptotic expansion, equation (2.4) are given by the solution to equations (2.7), (2.8) and (2.9). The appropriate boundary conditions for $\hat{p}_n$ are

$$\hat{p}_n\quad\text{is bounded as}\quad y\to\pm\infty. \tag{2.11}$$

For convenience a new similarity co-ordinate is introduced given by $\eta=y/s$, and the mean velocity field is taken to be a function of η only. If a local wavenumber and

frequency in the form $k_0 = \alpha s$ and $\beta = \omega s$ are defined, then the pressure fluctuation may be written in terms of η and β as

$$\hat{p}_0(\eta, \beta) = A_0(\beta)\, \xi(\eta, \beta) \tag{2.12}$$

and from equation (2.7) $\xi(\eta, \beta)$ satisfies the equation

$$L_\eta[\xi] = 0, \tag{2.13a}$$

where

$$L_\eta[\ ] \equiv \left[\frac{\partial^2}{\partial \eta^2} + \frac{2k_0}{\hat{\beta}} \frac{dU}{d\eta} \frac{\partial}{\partial \eta} - (k_0^2 - M^2 \hat{\beta}^2)\right] \tag{2.13b}$$

and

$$\hat{\beta} = \beta - k_0 U. \tag{2.13c}$$

The boundary conditions for ξ from equation (2.11) are

$$\xi \to 0 \quad \text{or bounded as} \quad \eta \to \pm \infty. \tag{2.14}$$

Equation (2.13) and boundary condition (2.14) form an eigenvalue problem. This is the identical problem that would have been obtained if the locally parallel flow approximation of classical hydrodynamic stability theory had been made. The eigenvalue is k_0. For $y \geqslant y_m$ equation (2.13) reduces to

$$\frac{\partial^2 \xi}{\partial \eta^2} - [k_0^2 - M^2(\beta - k_0)^2]\, \xi = 0. \tag{2.15}$$

The solution of equation (2.15) which satisfies the boundedness condition is

$$\xi = \exp[-\{k_0^2 - M^2(\beta - k_0)^2\}^{\frac{1}{2}} \eta] = \exp[-\lambda y],$$

where

$$\lambda = \{\alpha^2 - M^2(\omega - \alpha)^2\}^{\frac{1}{2}} \quad \text{and} \quad \mathrm{Re}\{\lambda\} > 0. \tag{2.16}$$

A normalization convection will be adopted for the eigenfunctions ξ by choosing the arbitrary multiplication constant in front of the exponential function of equation (2.16) to be unity. Equations (2.4), (2.12) and (2.16) lead to

$$p'(x, y, t) = A_0(s)\, e^{i\theta(x) - \lambda y - i\omega t} + O(\epsilon) \quad \text{for} \quad y \geqslant y_m. \tag{2.17}$$

Equation (2.8) may also be written in terms of the similarity co-ordinate. In order that a solution exists for the resulting equation it must satisfy the solvability condition; that is the inhomogeneous terms are orthogonal to every solution of the adjoint homogeneous problem [with an appropriate contour deformation in the η plane for damped waves (see appendix B and § 4)]. That is,

$$\int_{-\infty}^{\infty} \psi \chi_1 \, d\eta = 0, \tag{2.18}$$

where $\psi(\eta, \beta)$ is the solution to the adjoint homogeneous equation. It is readily verified that $\psi = \xi/\hat{\beta}^2$ so that equation (2.18) becomes,

$$\int_{-\infty}^{\infty} \frac{\xi \chi_1}{\hat{\beta}^2} d\eta = \int_{-\infty}^{\infty} \frac{\xi \chi_1}{\hat{\omega}^2} dy = 0. \tag{2.19}$$

This solvability condition leads to an ordinary differential equation for $A_0(\beta)$ in the form,

$$I_3 \frac{dA_0}{d\beta} + (I_4 + I_5)\, A_0 = 0, \tag{2.20}$$

where
$$I_3 = \int_{-\infty}^{\infty} \left[B_1 \xi + B_2 \frac{\partial \xi}{\partial \eta} \right] \psi d\eta, \tag{2.21a}$$

$$I_4 = \int_{-\infty}^{\infty} \left[B_1 \frac{\partial \xi}{\partial \beta} + B_2 \frac{\partial^2 \xi}{\partial \eta \, \partial \beta} \right] \psi d\eta \tag{2.21b}$$

and
$$I_5 = \int_{-\infty}^{\infty} \left\{ \left[B_3 \xi + B_4 \frac{\partial \xi}{\partial \eta} \right] \frac{dk_0}{d\beta} + B_5 \xi + B_6 \frac{\partial \xi}{\partial \eta} \right\} \psi d\eta, \tag{2.21c}$$

where the coefficients B_i are given in appendix A. Now with $\xi(\eta, s)$ to be obtained from the eigenvalue problem of equations (2.13) and (2.14) and $A_0(s)$ to be found by integrating equation (2.20), the slowly varying wave solution in the form

$$p'(x, y, t) = A_0(s)\, \xi(\eta, s)\, e^{i\theta(x) - i\omega t} + O(\epsilon), \tag{2.22}$$

is completely defined to order unity.

In evaluating the integrals of equation (2.21) the values of $dk_0/d\beta$ and $\partial \xi/\partial \beta$ may be obtained using a finite-difference calculation based on the values of k_0 and ξ at successive values of β. However, they may also be evaluated locally using the technique employed by Bouthier (1972, 1973) and Saric & Nayfeh (1975). Differentiating equation (2.13) with respect to β gives an inhomogeneous equation for $\partial \xi/\partial \beta$ of the form

$$L_\eta[\partial \xi/\partial \beta] = h_1 (dk_0/d\beta) + h_2, \tag{2.23}$$

where h_1 and h_2 are given in appendix A. Application of the solvability condition to equation (2.23) leads to an equation for $dk_0/d\beta$ and the inhomogeneous equation for $\partial \xi/\partial \beta$ may then be solved directly.

2.2. *Higher-order terms of the multiple-scales asymptotic expansion*

The higher-order terms of the multiple-scales asymptotic expansion (2.4) are given by the solution of the inhomogeneous equations (2.9). Since the corresponding homogeneous equation has an eigensolution, $\hat{\xi}$, each solution for $\hat{p}_n$ can be regarded as consisting of the sum of a particular solution and a complementary solution of the form $A_n(s)\, \hat{\xi}(y/s, s)$ where A_n is an unknown amplitude. This unknown amplitude may be determined in similar manner to A_0 from the solvability condition applied to χ_{n+1} in equation (2.9)

$$\int_{-\infty}^{\infty} \frac{\hat{\xi}(y, s)\, \chi_{n+1}}{\hat{\omega}^2} dy = 0, \quad n = 0, 1, 2, \ldots. \tag{2.24}$$

The above solvability condition leads to an ordinary differential equation for A_n. This equation can be integrated, at least numerically, so that the complementary solution is determined completely. The appropriate particular solutions may be obtained by the method of variation of parameters. For $y \geqslant y_m$ the eigenfunction $\hat{\xi}$ is given by equation (2.16). Another linearly independent solution of equation (2.15) is

$$\hat{\xi} = \exp\left[\{k_0^2 - M^2(\beta - k_0)^2\}^{\frac{1}{2}} \eta \right] = e^{\lambda y}. \tag{2.25}$$

Now let $\tilde{\xi}(y)$ be the solution of (2.7) which takes the form given by (2.25) for $y \geqslant y_m$. Then $\hat{\xi}(y)$ and $\tilde{\xi}(y)$ are two linearly independent solutions of the corresponding homogeneous equation of (2.9). It may be shown readily that the Wronskian $W(\hat{\xi}, \tilde{\xi})$ is given by

$$W(\hat{\xi}, \tilde{\xi}) = 2\lambda \hat{\omega}^2 / (\omega - \alpha)^2. \tag{2.26}$$

Applying the method of variation of parameters (see Boyce & DiPrima 1977, ch. 3) to (2.9) using ξ and $\bar{\xi}$ as the fundamental set of solutions, the complete solution is found to be

$$\hat{p}_n = A_n \xi(y,s) - \xi(y,s)\int_{-\infty}^{y} \frac{\bar{\xi}(t,s)\,\chi_n(t,s)}{W(\xi,\bar{\xi})}\,dt + \bar{\xi}(y,s)\int_{-\infty}^{y} \frac{\xi(t,s)\,\chi_n(t,s)}{W(\xi,\bar{\xi})}\,dt. \quad (2.27)$$

Using the explicit form of the Wronskian given in equation (2.26), equation (2.27) may be rewritten as

$$\hat{p}_n = A_n \xi(y,s) + \frac{(\omega-\alpha)^2}{2\lambda}\left[-\xi(y,s)\int_{-\infty}^{y} \frac{\bar{\xi}(t,s)\,\chi_n(t,s)}{\hat{\omega}^2}\,dt + \bar{\xi}(y,s)\int_{-\infty}^{y} \frac{\xi(t,s)\,\chi_n(t,s)}{\hat{\omega}^2}\,dt\right]. \quad (2.28)$$

The pressure $\hat{p}_n(y,s)$ as given by equation (2.28) clearly satisfies the boundedness condition as $y \to -\infty$. That the solution is bounded as $y \to +\infty$ is guaranteed by the solvability condition (2.24). The last term in (2.28) may be written in a more useful form using this solvability condition, that is,

$$\hat{p}_n = A_n \xi(y,s) - \frac{(\omega-\alpha)^2}{2\lambda}\left\{\xi(y,s)\int_{-\infty}^{y} \frac{\bar{\xi}(t,s)\,\chi_n}{\hat{\omega}^2}\,dt + \bar{\xi}(y,s)\int_{y}^{\infty} \frac{\xi(t,s)\,\chi_n}{\hat{\omega}^2}\,dt\right\}. \quad (2.29)$$

Equation (2.29) and the solvability condition (2.24) provide the complete solution of the amplitude functions of the slowly varying wave solution (2.4) to any order of the expansion parameter ϵ. Unfortunately, as will be shown below, this multiple-scales asymptotic expansion has only a limited range of validity.

2.3. *The singular perturbation problem*

In this section it will be shown that the multiple-scales asymptotic expansion (2.4) is not uniformly valid for large y. The region $y > y_m$, where the mean flow is uniform (i.e. $U = 1$, $V = 0$), will be examined. In this region the inhomogeneous terms of (2.9) are given explicitly by (2.10). The functions ξ and $\bar{\xi}$ of (2.29) take the following simple form

$$y > y_m, \quad \xi = e^{-\lambda y}, \quad \bar{\xi} = e^{\lambda y}, \quad (2.30)$$

so that the general expression for $\hat{p}_n$ becomes

$$\hat{p}_n(y,s) = D_n e^{-\lambda y} - \frac{e^{-\lambda y}}{2\lambda}\int^{y} e^{\lambda t}\bar{\chi}_n(t,s)\,dt - \frac{e^{\lambda y}}{2\lambda}\int_{y}^{\infty} e^{-\lambda t}\bar{\chi}_n\,dt, \quad \text{for} \quad y > y_m, \quad (2.31a)$$

where

$$D_n = A_n - \frac{1}{2\lambda}\left[(\omega-\alpha)^2\int_{-\infty}^{y_m} \frac{\bar{\xi}(t,s)\,\chi_n}{\hat{\omega}^2}\,dt + \int_{y_m} e^{\lambda t}\bar{\chi}_n(t,s)\,dt\right]. \quad (2.31b)$$

Equation (2.31) gives the dependence of $\hat{p}_n$ on y for $y > y_m$. It holds for all values of n provided χ_0 is taken to be zero.

With $\hat{p}_0 = A_0\xi = A_0\exp(-\lambda y)$ for $y \geqslant y_m$ the inhomogeneous term $\bar{\chi}_1$ may be computed from equation (2.10). This gives,

$$\bar{\chi}_1 = (C_1 + C_2 y)\,e^{-\lambda y}, \quad (2.32)$$

where

$$C_1 = -2i[M^2(\omega-\alpha)+\alpha]\,dA_0/ds - i(1-M^2)\,A_0\,d\alpha/ds$$

and

$$C_2 = 2i[M^2(\omega-\alpha)+\alpha]^2\frac{A_0}{\lambda}\frac{d\alpha}{ds}.$$

Substitution of equation (2.32) into equation (2.31a) and evaluating the various integrals it is found that for $y > y_m$

$$\hat{p}_1 = (B_{10} + B_{11}y + B_{12}y^2)\, e^{-\lambda y}, \tag{2.33}$$

where $$B_{10} = D_1 - \frac{1}{4\lambda^2}\left(C_1 + \frac{C_2}{2\lambda}\right), \quad B_{11} = -\frac{1}{2\lambda}\left(C_1 + \frac{C_2}{2\lambda}\right)$$

and $$B_{12} = -\frac{C_2}{4\lambda}.$$

Now that $\hat{p}_0$ and $\hat{p}_1$ are determined it is possible to find $\hat{p}_2$ in the same manner. After some computation it may be shown that,

$$\hat{p}_2 = [B_{20} + B_{21}y + B_{22}y^2 + B_{23}y^3 + B_{24}y^4]\, e^{-\lambda y}. \tag{2.34}$$

The expressions for the coefficients B_{2i} are rather complicated and will not be written out. Only the dependence of the solution on y is of interest. By continuing this process or by mathematical induction it may be shown that,

$$\hat{p}_n \sim B_{2,2n}\, y^{2n} e^{-\lambda y} \quad \text{as} \quad y \to \infty. \tag{2.35}$$

Thus for large y the multiple scales asymptotic expansion (2.4) behaves like,

$$p'(x, y, t) \sim \sum_{n=0}^{\infty} K_n\, \epsilon^n y^{2n} e^{-\lambda y + i\theta(x) - i\omega t} \quad \text{as} \quad y \to \infty, \tag{2.36}$$

where K_n are functions of x alone. Owing to the appearance of $\epsilon^n y^{2n} \exp[-\lambda y]$ in the higher-order terms, the asymptotic expansion does not hold for $y \gg \epsilon^{-\frac{1}{2}}$. In other words the multiple-scales expansion is non-uniformly valid. As far as is known no single asymptotic expansion which is uniformly valid for all y can be constructed for the present problem. Van Dyke (1975) states on page 33 of his book 'a singular perturbation problem is best defined as one in which no single asymptotic expansion is uniformly valid throughout the field of interest'. Thus the present perturbation problem is unfortunately singular.

3. Continuation of the instability-wave solution into the region $y > y_m$

It is now necessary to construct an extension of the multiple-scales asymptotic expansion which is uniformly valid for $y > y_m$ in the upper half plane. To do this it will be first determined what this extended solution ought to satisfy. The disturbances associated with the instability wave are governed by the linearized continuity, momentum and energy equations and the equation of state, namely, equations (2.1) and (2.2). These are, of course, the same equations that were used to determine the multiple-scales slowly-varying wave solution. However in the region $y > y_m$, U is unity and V is zero so that these equations simplify to

$$y > y_m, \quad \frac{\partial p_e}{\partial t} + \frac{\partial p_e}{\partial x} + \gamma\left(\frac{\partial u_e}{\partial x} + \frac{\partial v_e}{\partial y}\right) = 0, \tag{3.1a}$$

$$\gamma M^2\left(\frac{\partial u_e}{\partial t} + \frac{\partial u_e}{\partial x}\right) = -\frac{\partial p_e}{\partial x} \tag{3.1b}$$

and $$\gamma M^2\left(\frac{\partial v_e}{\partial t} + \frac{\partial v_e}{\partial x}\right) = -\frac{\partial p_e}{\partial y}. \tag{3.1c}$$

The subscript e indicates that the variables are the extended solution in the region $y > y_m$. Eliminating u_e and v_e from equation (3.1) the governing equation for p_e is found to be

$$M^2\left(\frac{\partial}{\partial t}+\frac{\partial}{\partial x}\right)^2 p_e-\left(\frac{\partial^2}{\partial x^2}+\frac{\partial^2}{\partial y^2}\right)p_e = 0. \tag{3.2}$$

The appropriate boundary condition for p_e at large y is the radiation or boundedness condition

$$y\to\infty, \quad p_e \text{ is bounded or behaves like outgoing waves.} \tag{3.3}$$

At this stage an inner boundary condition is needed for p_e in the region y slightly greater than y_m. For the case $\epsilon = 0$ the multiple scales asymptotic expansion (2.4) truncates (only one term is needed for a truly parallel mean flow) so that the expansion converges for all values of y. It will be assumed that the expansion also converges for some value of y slightly greater than $y = y_m$ even when ϵ has a small but finite value. If this convergence is realized then, by appealing to the concept of analytic continuation, the natural inner boundary condition for the extended solution p_e is that it must be identically equal to the convergent asymptotic expansion. Under these circumstances p_e is the analytic continuation of p'. This leads to the inner boundary condition,

$$p_e = \left\{\sum_{n=0}^{\infty}\epsilon^n\hat{p}_n(y,s)\right\}e^{i\theta(x)-i\omega t} \quad \text{(for } y \text{ slightly greater than } y_m\text{)}, \tag{3.4}$$

where $p_n(y,s)$; $n = 0, 1, 2, \ldots$ are given by equation (2.31).

Summarizing, the extended solution p_e must satisfy equation (3.2), the radiation and inner boundary conditions (3.3) and (3.4) and be uniformly valid for all $y > y_m$.

3.1. *The extended problem*

It will now be shown that the extended solution, p_e as defined by equations (3.2), (3.3) and (3.4) is identical to the solution ϕ of the following boundary-value problem:

$$\text{for} \quad y \geqslant 0, \quad M^2\left(\frac{\partial}{\partial t}+\frac{\partial}{\partial x}\right)^2\phi-\left(\frac{\partial^2\phi}{\partial x^2}+\frac{\partial^2\phi}{\partial y^2}\right) = 0; \tag{3.5}$$

$$\text{as} \quad y\to\infty, \quad \phi \text{ satisfies the radiation or boundedness condition;} \tag{3.6}$$

$$\text{on} \quad y = 0, \quad \phi = \sum_{n=0}^{\infty}\epsilon^n g_n(\epsilon x)\,e^{i\theta(x)-i\omega t}. \tag{3.7}$$

Here $g_n(s)$, $s = \epsilon x$, will be related to the multiple scales expansion (2.4) below. Equations (3.5), (3.6) and (3.7) constitute a well-defined boundary-value problem whose solution is *unique*. Since equations (3.5) and (3.6) are identical to equations (3.2) and (3.3) the hypothesis that $\phi = p_e$ for $y > y_m$ could be proved if it could be shown that ϕ possesses an asymptotic expansion which is identical to the right-hand side of equation (3.4) for y slightly greater than y_m. To show this the above boundary-value problem will be solved for ϕ explicitly in the form of a multiple-scales asymptotic expansion. Let ϕ be given by

$$\phi(x,y,t) = \sum_{n=0}^{\infty}\epsilon^n\phi_n(y,s)\,e^{i\theta(x)-i\omega t}. \tag{3.8}$$

Substitution of (3.8) into (3.5) and partitioning terms by powers of ϵ leads to the following set of equations:

$$\partial^2\phi_n/\partial y^2 - [\alpha^2 - M^2(\omega-\alpha)^2]\,\phi_n = \bar{\chi}_n(\phi_{n-1}, \phi_{n-2}) \quad n = 0, 1, 2, \ldots, \tag{3.9}$$

where $\phi_{-2} = \phi_{-1} = 0$ and the functional form of $\bar{\chi}_n(\phi_{n-1}, \phi_{n-2})$ is given by (2.10). The boundary conditions on ϕ_n are found in (3.6) and (3.7), namely

$$\text{as} \quad y \to \infty, \quad \phi_n \text{ is bounded}, \tag{3.10}$$

$$\text{on} \quad y = 0, \quad \phi_n = g_n(s). \tag{3.11}$$

Two linearly independent solutions of the corresponding homogeneous equations of (3.9) are, $\exp[-\lambda y]$ and $\exp[\lambda y]$ where λ is given by (2.16). For $n = 0$, $\bar{\chi}_0 = 0$ in (3.9) so that the solution ϕ_0 which satisfies boundary conditions (3.10) and (3.11) may easily be shown to be

$$\phi_0 = g_0(s)\, e^{-\lambda y}. \tag{3.12}$$

For $n \geqslant 1$ the solution of the inhomogeneous equation (3.9) and boundary conditions (3.10) and (3.11) may again be determined by the method of variation of parameters. It is readily shown that

$$\phi_n = \left[g_n(s) + \frac{1}{2\lambda}\left\{\int_0^\infty e^{-\lambda t}\bar{\chi}_n\, dt - \int_0 e^{\lambda t}\bar{\chi}_n\, dt\right\}\right] e^{-\lambda y} - \frac{e^{-\lambda y}}{2\lambda}\int^y e^{\lambda t}\bar{\chi}_n\, dt - \frac{e^{\lambda y}}{2\lambda}\int_y^\infty e^{-\lambda t}\bar{\chi}_n\, dt. \tag{3.13}$$

Now setting

$$g_0(s) = A_0(s) \tag{3.14a}$$

and for $n \geqslant 1$,

$$g_n(s) = A_n(s) - \frac{1}{2\lambda}\left[(\omega-\alpha)^2\int_{-\infty}^{y_m} \frac{\hat{\xi}(t,s)\,\chi_n(t,s)}{\hat{\omega}^2}\, dt - \int_0^{y_m} e^{\lambda t}\bar{\chi}_n\, dt + \int_0^\infty e^{-\lambda t}\bar{\chi}_n\, dt\right], \tag{3.14b}$$

the two expressions on the right-hand sides of (2.31) and (3.13) are identical. Thus $\phi_n = \hat{p}_n$ in the region y slightly greater than y_m. That is, ϕ satisfies the inner boundary condition (3.4). Thus the extended solution p_e is equal to the solution ϕ (for $y \geqslant y_m$) of the boundary-value problem defined by (3.5), (3.6) and (3.7).

3.2. *Uniformly-valid asymptotic expansion of the extended problem*

Having shown that the extended solution, p_e, is given by the solution of the boundary-value problem defined by (3.5), (3.6) and (3.7) a uniformly valid expansion of the extended solution for $y > y_m$ is constructed. The solution of the boundary-value problem (3.5) to (3.7) is unique. However different methods of solution would yield solutions of different forms which may or may not be uniformly valid for $y > y_m$. At large distances from the mixing layer the disturbances mainly consist of acoustic waves. Unlike waves in the mixing layer whose amplitude changes slowly in the x direction as compared with the y variation the acoustic waves have no such distinction. Thus to seek a solution valid for large y the slow variable $s = \epsilon x$ must not be used, rather x and y must be treated on an equal footing. Thus a solution will be sought by the method of Fourier transforms.

The Fourier transform and its inverse are defined by

$$\bar{f}(k) = 1/2\pi\int_{-\infty}^{\infty} f(x)\, e^{-ikx}\, dx; \quad f(x) = \int_{-\infty}^{\infty} \bar{f}(k)\, e^{ikx}\, dk. \tag{3.15}$$

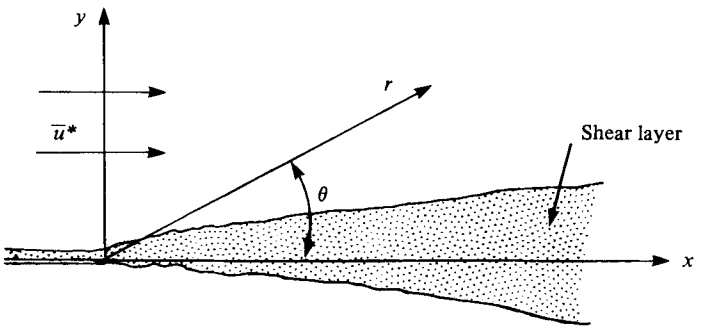

FIGURE 2. Co-ordinates for acoustic far-field solution.

Applying the Fourier transform to (3.5) to (3.7) and setting $\phi = \hat{\phi}(x,y)\exp[-i\omega t]$ it is easy to find that the Fourier transform of $\hat{\phi}$, $\bar{\phi}$, is given by the solution of

$$d^2\bar{\phi}/dy^2 + [M^2(\omega-k)^2 - k^2]\bar{\phi} = 0 \tag{3.16}$$

and, at $y = 0$,

$$\bar{\phi} = \sum_{n=0}^{\infty} \epsilon^n \bar{g}_n(k), \tag{3.17}$$

where

$$\bar{g}_n(k) = 1/2\pi \int_{-\infty}^{\infty} g_n(\epsilon x)\, e^{i\theta(x)-ikx}\, dx. \tag{3.18}$$

The solution of (3.16) and (3.17) which also satisfies the radiation condition is

$$\bar{\phi} = \sum_{n=0}^{\infty} \epsilon^n \bar{g}_n(k) \exp[iM\omega\{(1-k/\omega)^2 - (k/M\omega)^2\}^{\frac{1}{2}} y], \tag{3.19a}$$

where

$$\mathrm{Re}\,\{(1-k/\omega)^2 - (k/M\omega)^2\}^{\frac{1}{2}} > 0. \tag{3.19b}$$

If $\mathrm{Re}\,\{[1-k/\omega)^2 - (k/M\omega)^2]^{\frac{1}{2}}\} = 0$ use the branch $\mathrm{Im}\,\{[(1-k/\omega)^2 - (k/M\omega)^2]^{\frac{1}{2}}\} > 0$. Performing the inverse Fourier transform leads to

$$\phi(x,y,t) = \sum_{n=0}^{\infty} \epsilon^n \int_{-\infty}^{\infty} \bar{g}_n(k) \exp[iM\omega\{(1-k/\omega)^2 - (k/M\omega)^2\}^{\frac{1}{2}} y + ikx - i\omega t]\, dk. \tag{3.20}$$

Clearly equation (3.20) is uniformly valid for all y (see also (3.22) below). Therefore it provides the proper continuation of the mixing-layer slowly-varying instability-wave solution to the region $y > y_m$ in the upper half plane.

3.3. *Acoustic far-field solution*

The sound radiation associated with the instability wave can be found by evaluating the integrals of equation (3.20). In evaluating the far-field solution polar co-ordinates (r,θ) will be used as shown in figure 2, where $x = r\cos\theta$, $y = r\sin\theta$. Equation (3.20) may be rewritten as (noting that ϕ is the fluctuating pressure which will be written as p)

$$p(r,\theta,t) = \sum_{n=0}^{\infty} \epsilon^n \int_{-\infty}^{\infty} \bar{g}_n(k) \exp[i([M^2(\omega-k)^2 - k^2]^{\frac{1}{2}} \sin\theta + k\cos\theta)\, r - i\omega t]\, dk. \tag{3.21}$$

In the limit $r \to \infty$, the integral can be evaluated by the method of stationary phase. This gives,

$$p(r,\theta,t) \underset{r\to\infty}{\sim} \left(\frac{2\pi M\omega}{r}\right)^{\frac{1}{2}} \frac{\sin\theta}{(1-M^2\sin^2\theta)^{\frac{3}{4}}} \left[\sum_{n=0}^{\infty} \epsilon^n \bar{g}_n(k_s)\right] \times \exp\left[i\omega(M[1-M^2\sin^2\theta]^{\frac{1}{2}} - M^2\cos\theta)(1-M^2)^{-1}r\right] \exp\left[-i\omega t - \tfrac{1}{4}i\pi\right], \quad (3.22)$$

where

$$k_s = \frac{M\omega}{(1-M^2)}\left\{\frac{\cos\theta}{(1-M^2\sin^2\theta)^{\frac{1}{2}}} - M\right\},$$

from which the directivity pattern of acoustic radiation, $D(\theta)$, can be calculated:

$$D(\theta) = \lim_{r\to\infty} \tfrac{1}{2}r|p|^2 = \frac{\pi M\omega}{(1-M^2\sin^2\theta)^{\frac{3}{2}}} \left|\sum_{n=0}^{\infty} \epsilon^n \bar{g}_n(k_s)\right|^2 \sin^2\theta. \quad (3.23)$$

Since ϵ is small, for practical purposes only the first term of the sum in equation (3.23) matters. From equations (3.14) and (3.18)

$$g_0(\epsilon x) = A_0(\epsilon x), \quad \bar{g}_0(k) = 1/2\pi \int_{-\infty}^{\infty} A_0(\epsilon x)\, e^{i\theta(x)-ikx}\, dx. \quad (3.24)$$

This finally leads to

$$D(\theta) \simeq \frac{\pi M\omega}{(1-M^2\sin^2\theta)^{\frac{3}{2}}} |\bar{g}_0(k_s)|^2 \sin^2\theta, \quad (3.25)$$

for: $0 \leqslant \theta \leqslant \pi$, if $M < 1$; $0 \leqslant \theta < \sin^{-1}[M^{-1}]$ if $M > 1$.

Similarly it is straightforward to show that the directivity pattern of acoustic radiation in the lower half-plane or stationary medium, to the zeroth order, is

$$D(\theta) = \pi\omega M |\bar{g}_0(\omega M\cos\theta)|^2 \sin^2\theta, \quad (3.26)$$

for $-\pi < \theta \leqslant 0$.

4. Numerical results

In this section the results for the instability-wave characteristics and the far-field noise radiation are presented. The mean velocity and the numerical procedure for calculating the disturbance growth by the method of multiple scales are described. The properties of damped inviscid waves are also discussed. Calculations are presented for both subsonic and supersonic free-stream Mach numbers.

4.1. *The instability-wave solution*

The mean velocity. The description of the mean velocity is based on experimental measurements in turbulent shear layers. The axial and transverse mean velocities are given by

$$U = \begin{cases} 0, & (\eta-\eta_0) \leqslant -6{\cdot}0, \\ 0{\cdot}5[1+\mathrm{erf}\,(\eta-\eta_0)], & -6{\cdot}0 < (\eta-\eta_0) < 6{\cdot}0, \\ 1, & (\eta-\eta_0) \geqslant 6{\cdot}0, \end{cases} \quad (4.1)$$

and

$$V = \begin{cases} 0{\cdot}5\eta_0[\mathrm{erf}\,(\eta-\eta_0)-1] - \exp\left[-(\eta-\eta_0)^2\right]/2\pi^{\frac{1}{2}}, & (\eta-\eta_0) < 6{\cdot}0, \\ 0, & (\eta-\eta_0) \geqslant 6{\cdot}0. \end{cases} \quad (4.2)$$

The complementary error-function profile (4.1) was found to provide a good fit to the axial velocity distribution for a wide range of Mach numbers in the initial mixing

region of a round jet by Lau, Morris & Fisher (1976). The value of η_0, which gives the location of the dividing streamline, is taken from Patel (1973) to be $-0{\cdot}3$. The rate of spread of an isothermal mixing layer is a function of the free-stream Mach number. Since the perturbation parameter, ϵ, in the present problem represents the rate of spread it will be a function of Mach number. The variation of ϵ with M is taken from Lau *et al.* (1976) and is given by

$$\epsilon = (0{\cdot}165 - 0{\cdot}045M^2)/\pi^{\frac{1}{2}}. \tag{4.3}$$

Numerical calculation procedure. With the mean velocity profiles defined the amplitude of the pressure fluctuation associated with the instability wave may be calculated above and below the layer. Firstly the 'parallel flow approximation' given by equation (2.13) is solved, subject to the boundary conditions (2.14). The form of the solution in the uniform and stationary fluid above and below the layer respectively are easily obtained:

$$\xi \sim e^{-\lambda_+ \eta} \quad \text{as} \quad \eta \to +\infty \tag{4.4a}$$

and

$$\xi \sim e^{\lambda_- \eta} \quad \text{as} \quad \eta \to -\infty, \tag{4.4b}$$

where

$$\lambda_+ = (k_0^2 - M^2(\beta - k_0)^2)^{\frac{1}{2}}, \tag{4.4c}$$

and

$$\lambda_- = (k_0^2 - M^2\beta^2)^{\frac{1}{2}}; \tag{4.4d}$$

$$\mathrm{Re}\{\lambda_\pm\} > 0.$$

The numerical integration is started above the layer and proceeds across the layer to $\mathrm{Re}(\eta) = 0$. A second integration is started below the shear layer and continues to $\mathrm{Re}(\eta) = 0$, where the two solutions are matched. The matching of the two solutions leads to a determinant which must be equal to zero to obtain the eigensolution. In practice this is done by minimizing the absolute value of the determinant. The contour of integration as discussed in appendix B must always be below the critical point, η_c, where $U = \beta/k_0$, for the mean velocity profile, equation (4.1), so that the damped inviscid solutions are correctly obtained. The indentation of the integration contour in the complex η plane lies on three straight lines joining the points, $[\mathrm{Re}(\eta_c) - 1, 0]$, $[\mathrm{Re}(\eta_c) - 1, \mathrm{Im}(\eta_c) - 1]$, $[\mathrm{Re}(\eta_c) + 1, \mathrm{Im}(\eta_c) - 1]$, and $[\mathrm{Re}(\eta_c) + 1, 0]$. The indentation of the contour into the complex η plane occurs whenever $\mathrm{Im}(\eta_c) < +1$. Further discussion of the damped inviscid solutions is given in appendix B and §4.2. An inverse Lagrangian interpolation is used to minimize the determinant in the eigenvalue search. Once the eigenvalue is found the eigenfunction, ξ, hence, the adjoint solution, ψ, is readily obtained since $\psi = \xi/\hat{\beta}^2$. The eigenfunction is normalized such that $\xi = e^{-\lambda_+ \eta}$ above the layer. The terms, h_1 and h_2 of equation (2.23) are then calculated and $dk_0/d\beta$ is given by

$$\frac{dk_0}{d\beta} = -\int_{-\infty}^{\infty} h_2 \psi d\eta \Big/ \int_{-\infty}^{\infty} h_1 \psi d\eta = -I_2/I_1. \tag{4.5}$$

The solution of the inhomogeneous equation for $\partial\xi/\partial\beta$, equation (2.23), is then calculated using the same integration contour and the integrals in (2.21) may also be found. Equation (2.21) may then be used to evaluate $A^{-1}dA/d\beta$.

Above the layer the solution for the fluctuating pressure may be written

$$p'(\eta, \beta) = A(\beta)\, e^{-\lambda_+ \eta + i\theta(x) - i\omega t}, \tag{4.6a}$$

	Exact solution	Numerical solution
k_0	1·0	$(1{\cdot}0000 + 1{\cdot}5377 \times 10^{-5}i)$
I_1	$-(4+2\pi i)$	$-(4{\cdot}0003 + 6{\cdot}2832i)$
I_2	$4\pi i$	$(5{\cdot}4219 \times 10^{-4} + 12{\cdot}566i)$
$dk_0/d\beta$	$\dfrac{2\pi(\pi+2i)}{(4+\pi^2)}$	$(1{\cdot}4232 + 0{\cdot}9060i)$

TABLE 1. Comparison of exact and numerical solutions, $\beta = 0{\cdot}5$.

and below the layer the solution is

$$p'(\eta,\beta) = C(\beta)\,A(\beta)\,e^{\lambda_-\eta + i\theta(x) - i\omega t}. \tag{4.6b}$$

Thus the corresponding equivalent rates of change of the pressure are given by

$$\left\{\frac{1}{p'}\frac{\partial p'}{\partial x}\right\}_{\text{above}} = i\alpha + \frac{\epsilon\omega}{A}\frac{dA}{d\beta} - \frac{\epsilon y}{\lambda_+}[\alpha + M^2(\omega-\alpha)]\left(\omega\frac{dk_0}{d\beta} - \alpha\right), \tag{4.7a}$$

$$\left\{\frac{1}{p'}\frac{\partial p'}{\partial x}\right\}_{\text{below}} = i\alpha + \epsilon\omega\left[\frac{1}{A}\frac{dA}{d\beta} + \frac{1}{C}\frac{dC}{d\beta}\right] + \frac{\epsilon\alpha y}{\lambda_-}\left(\omega\frac{dk_0}{d\beta} - \alpha\right). \tag{4.7b}$$

The growth rates of the pressure fluctuation are clearly functions of distance from the layer, y. This functional dependence is due to the changing shape of the eigenfunctions with downstream distance. However the effect of the last term in equation (4.7) is negligible if regions close to the edge of the layer are considered. The growth rate and wavenumber of the slightly diverging flow are then given respectively by the real and imaginary parts of the remaining terms of the right-hand side of equations (4.7), that is

$$i\alpha_+ \simeq i\alpha + \frac{\epsilon\omega}{A}\frac{dA}{d\beta} \tag{4.8a}$$

and

$$i\alpha_- \simeq i\alpha_+ + \frac{\epsilon\omega}{C}\frac{dC}{d\beta}. \tag{4.8b}$$

Numerical accuracy. As a first check on the numerical accuracy of the calculation method, the numerical results were compared with a known exact solution. For a mean velocity profile of the form

$$U = 0{\cdot}5[1 + \tanh(\eta - \eta_0)], \tag{4.9}$$

the eigensolution, using the normalization employed above is

$$k = 1{\cdot}0, \quad \beta = 0{\cdot}5, \quad M = 0{\cdot}0,$$

$$\xi = 0{\cdot}5\,\mathrm{sech}\,(\eta - \eta_0),$$

$$\psi = 2\,\mathrm{sech}\,(\eta-\eta_0)/\tanh^2(\eta-\eta_0).$$

The integrals in equation (4.5) may then be evaluated analytically. The comparison of the numerical and analytical solutions are shown in table 1.

Numerical calculations of the instability wave solution have been performed for the incompressible case, $M = 0$, and for $M = 0{\cdot}75$, 1·25 and 1·75. The 'parallel flow approximation' to the local growth rate, given by $-\mathrm{Im}\{k_0\}$ is shown in figure 3 as a

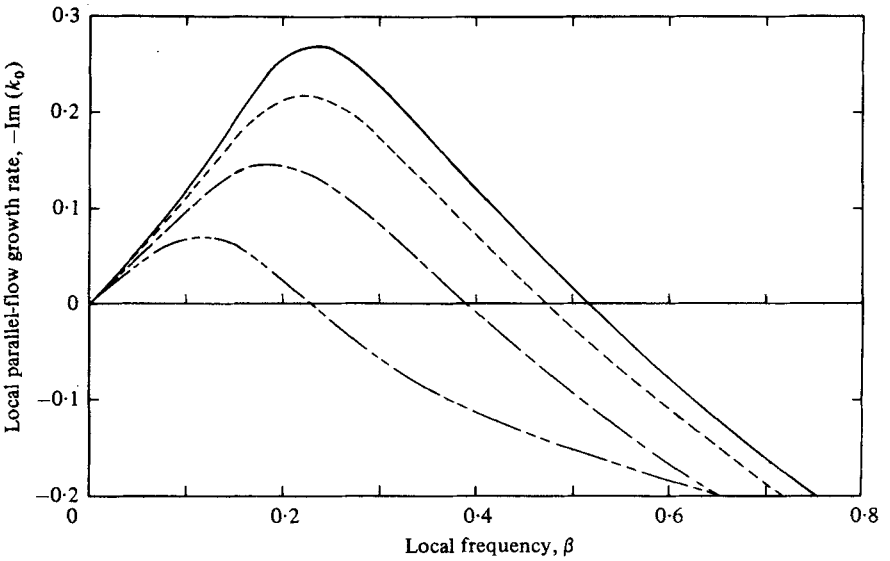

FIGURE 3. Variation of local parallel-flow growth rate with local frequency. —, $M = 0$; · · · ·, $M = 0{\cdot}75$; – – –, $M = 1{\cdot}25$; – · – · –, $M = 1{\cdot}75$.

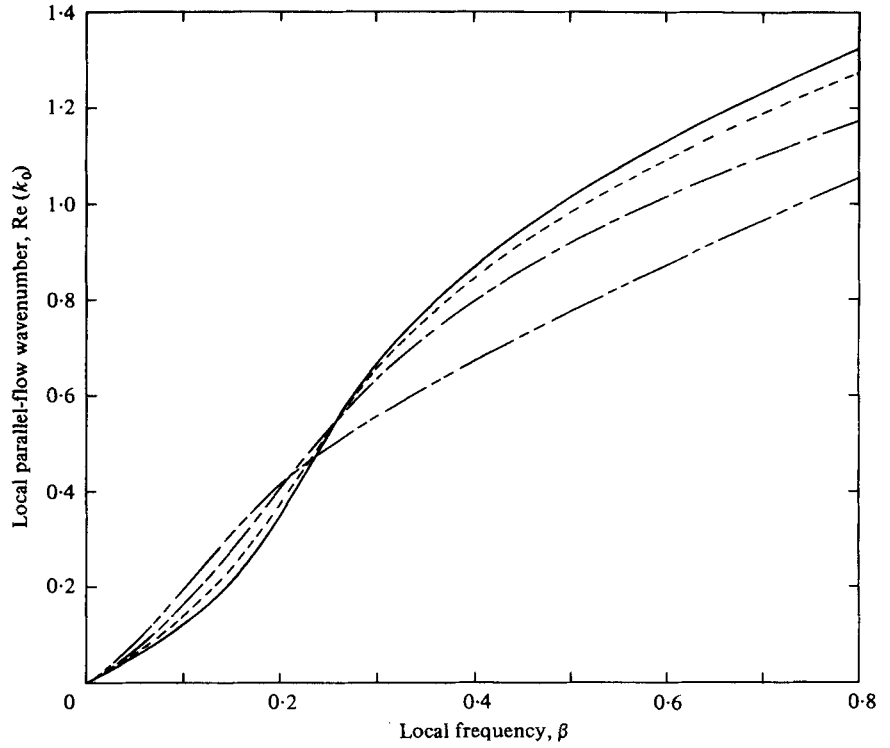

FIGURE 4. Variation of local parallel-flow wavenumber with local frequency. For symbols see figure 3.

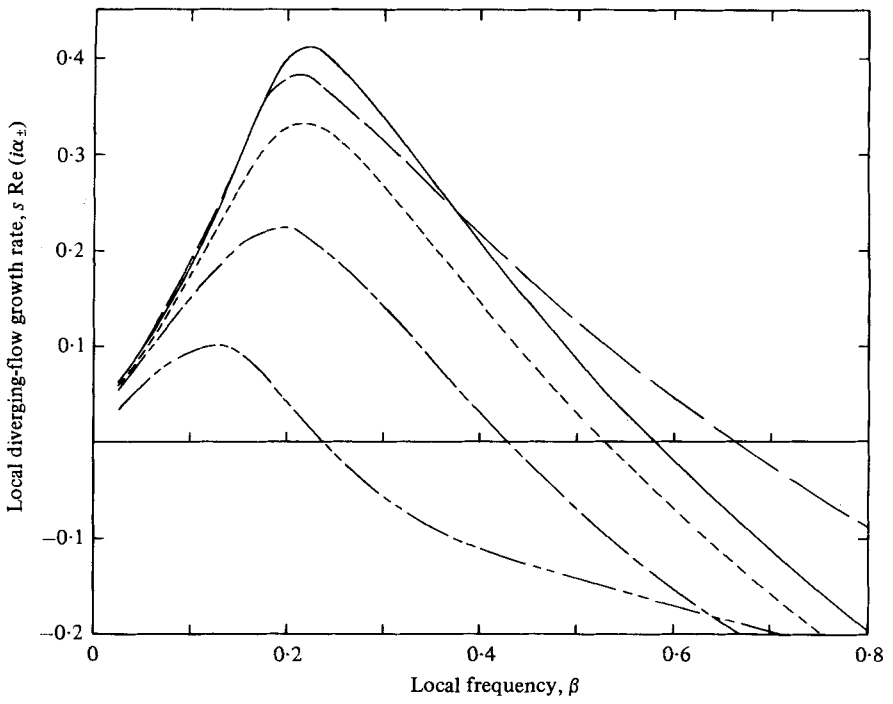

FIGURE 5. Variation of local 'diverging-flow' growth rate with local frequency. Below layer: ——, $M = 0$; · · · · ·, $M = 0{\cdot}75$; – – –, $M = 1{\cdot}25$; – · – · –, $M = 1{\cdot}75$. Above layer: ——, $M = 0$.

function of the free-stream Mach number. It should be noted that in the parallel flow approximation the growth rate is independent of the transverse location in the shear layer. As the free-stream Mach number increases the local growth rate decreases. This was also noted by Gropengieser (1969) and Michalke (1971). The variation of the parallel flow approximation wave number is shown in figure 4. At lower frequencies increasing the Mach number increases the local wavenumber which results in a decrease in the phase velocity. The reverse occurs at higher local frequencies though in this region the waves are decaying. The local growth rates which are determined from equation (4.8) are shown in figure 5. The divergence of the flow is seen, by comparison with figure 3, to increase the growth rate. The maximum growth rate for the pressure below the layer for $M = 0$, is 50 per cent higher than the maximum growth rate obtained using the locally parallel flow approximation. The growth rates above and below the layer are shown for the $M = 0$ case only. The pressure wave above the layer is seen to grow for a broader range of local frequencies (thicknesses) though the maximum growth rate is greatest below the shear layer. The 'diverging-flow' wavenumbers are shown as a function of local frequency in figure 6. At high frequencies the flow divergence increases the wavenumber and hence reduces the phase velocity. At low frequencies there is a reduction in the local wavenumber which results in the occurrence of very high phase velocities. There is an indication that at sufficiently low local frequencies and Mach numbers upstream wave propagation may occur.

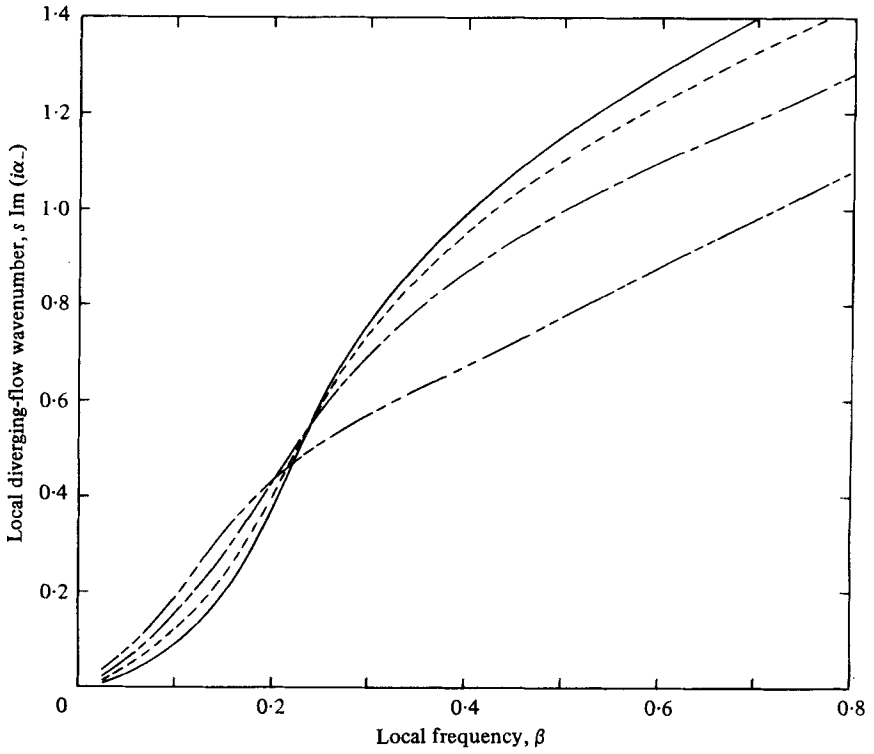

FIGURE 6. Variation of local 'diverging-flow' wavenumber with local frequency below the shear layer. For symbols see figure 3.

4.2. *Inviscid damped wave solution*

It has been suggested that in a slowly-varying inviscid flow only the growth of waves can be followed and that for decaying modes there may not exist any continuous solution to the inviscid equations of parallel flow (Lin 1955, ch. 8; Betchov & Criminale 1967, p. 80). In appendix B the correct procedure for constructing the inviscid damped wave solution is discussed. In order to demonstrate that the damped inviscid solutions obtained by analytic continuation in the complex plane as described in appendix B and above are valid for this problem the corresponding viscous flow analysis will be performed for the incompressible, $M = 0$, case. It will be shown that the viscous solutions tend to the inviscid solution as the Reynolds number increases for damped viscous and inviscid waves.

The linearized viscous equations corresponding to the inviscid equations (2.6) for the zeroth-order fluctuations (or the parallel flow approximations) for incompressible flow are,

$$ik_0\hat{u}_0 + \hat{v}_0' = 0, \tag{4.10a}$$

$$-i\hat{\beta}\hat{u}_0 + \frac{dU}{d\eta}\hat{v}_0 + ik_0\hat{p}_0 = \frac{1}{R}\{\hat{u}_0'' - k_0^2\hat{u}_0\} \tag{4.10b}$$

and

$$-i\hat{\beta}\hat{v}_0 + \hat{p}_0' = \frac{1}{R}\{\hat{v}_0'' - k_0^2\hat{v}_0\}, \tag{4.10c}$$

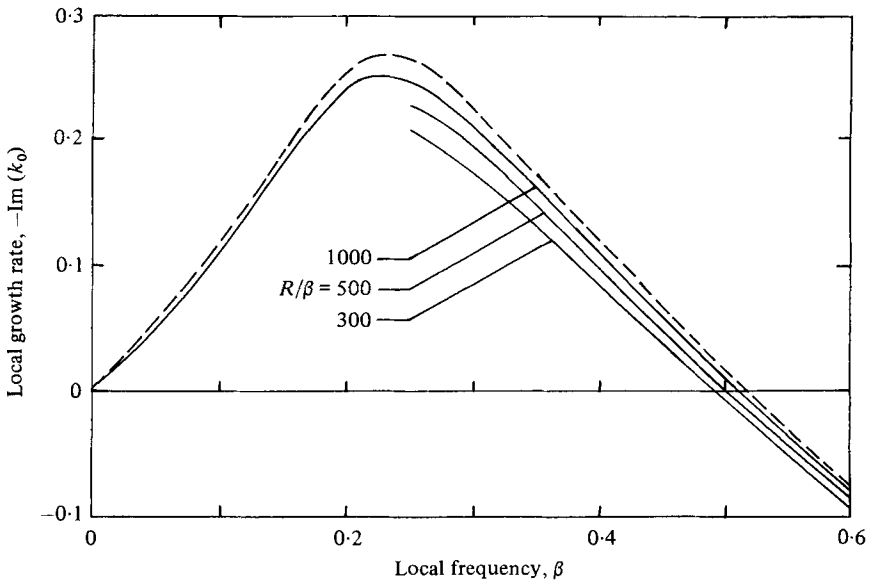

FIGURE 7. Effect of Reynolds number on growth rate, $M = 0$. ----, inviscid solution.

where the local Reynolds number, $R = \bar{u}^* s/\nu$. This set of simultaneous equations may be solved directly for the eigenvalue k_0 and the functions $\hat{u}_0$, $\hat{v}_0$ and $\hat{p}_0$. In the present analysis a single fourth-order equation for $\hat{v}_0$ (the Orr–Sommerfeld equation) was obtained in the form,

$$\beta(\hat{v}_0'' - k_0^2 \hat{v}_0) + k_0 \frac{d^2U}{d\eta^2}\hat{v}_0 = \frac{1}{iR}\{\hat{v}_0^{\mathrm{iv}} - 2k_0^2 \hat{v}_0'' + k_0^4 \hat{v}_0\}. \tag{4.11}$$

Equation (4.11) may be integrated numerically subject to the boundary conditions

$$\hat{v}_0 = \hat{v}_0' \to 0 \quad \text{as} \quad \eta \to \pm\infty. \tag{4.12}$$

The eigenfunction for the pressure can be obtained in terms of $\hat{v}_0$ and its derivatives from (4.10). The linear independence of the solutions is preserved using an orthonormalization procedure at a number of steps within the range of the numerical integration. The numerical procedure is the same as that used by Morris (1976*b*). The calculated growth rate, $-\mathrm{Im}\,(k_0)$, is shown in figure 7 for several values of Reynolds number. The corresponding variations in the real part of the wavenumber, $\mathrm{Re}\,(k_0)$, are shown in figure 8. As the Reynolds number increases so the eigenvalues approach the inviscid solution. This is the case for both growing and damped waves. However, in the present analysis, it is the eigenfunction that must be calculated in order to evaluate the integrals required in the multiple-scales asymptotic solution. In order to compare the inviscid and viscous solutions for damped waves over the entire range of integration the viscous solution was obtained by integrating on the same contour in the complex η plane as used in the inviscid solution. The viscous eigenfunction obtained on the complex contour was found to be identical to that obtained by integration along the real η axis where the two contours were coincident. The eigenfunction obtained for a Reynolds number, $R/\beta = 500$, and a local frequency, $\beta = 0{\cdot}6$ (which corresponds to a damped wave) is compared with the corresponding inviscid solution in figure 9. Parts

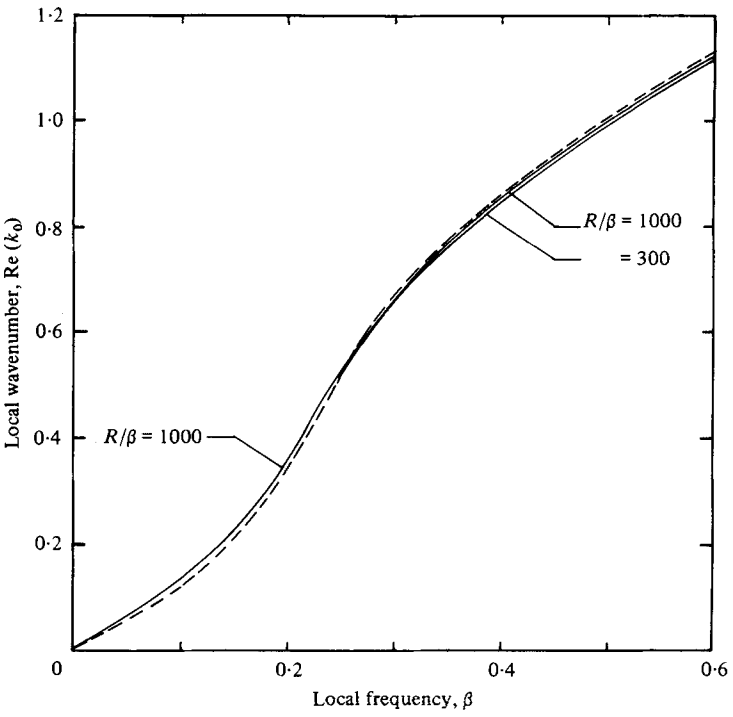

FIGURE 8. Effect of Reynolds number on the real part of the wavenumber, $M = 0$. - - - -, inviscid solution.

(a) and (e) of the Figure are on the real η axis and parts (b), (c) and (d) are in the complex η plane. The eigenfunctions are both normalized such that $\xi = \exp[-k_0\eta]$ at $\eta = 6{\cdot}0$ which is the upper limit of the numerical integration. The two solutions, viscous and inviscid, are almost identical, the difference being almost impossible to show graphically. Typical values for the two solutions are given in table 2 at various locations on the complex contour. Thus we have shown that the inviscid analysis provides a valid approximation to the viscous analysis, for even moderate local Reynolds numbers, and that the validity of this approximation includes damped inviscid waves.

Now that it has been shown that the inviscid-wave model is valid during both the growth and decay of the wave in the present analysis, the far field noise radiation, which is intimately connected with this growth and decay process, will be calculated in the next section.

4.3. *Far-field noise radiation*

In § 3 it was shown how the multiple scales expansion for the pressure fluctuations in the shear layer may be extended into the acoustic far field. The wavenumber component spectrum of these fluctuations in the near field will now be examined and the far-field directivity patterns for both subsonic and supersonic free-stream velocities will be calculated.

The far-field noise radiation, given in (3.25) and (3.26) is seen to depend on the amplitude of $\bar{g}_0(k)$ evaluated at the stationary point of the integral of (3.21) (for radiation into the uniform stream). $\bar{g}_0(k)$ is the Fourier transform of the quantity $A_0(\epsilon x)\exp[i\theta(x)]$ and may be regarded as the wavenumber component spectrum

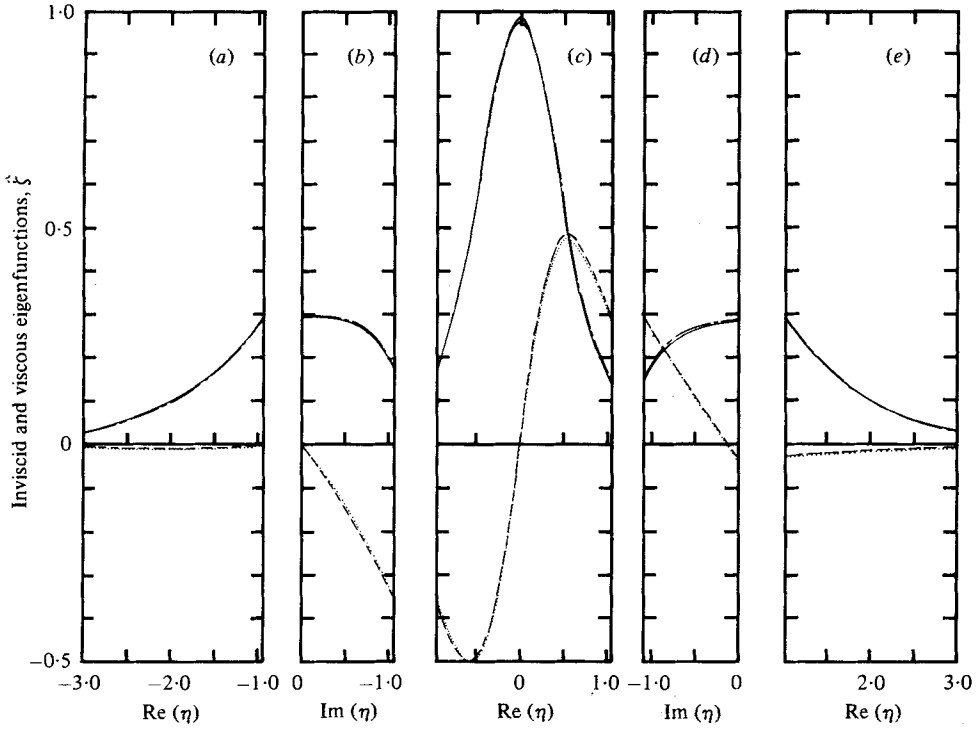

FIGURE 9. Comparison of viscous and inviscid eigenfunctions, $M = 0$, $R = 300$, $\beta = 0{\cdot}6$. (*a*) $\mathrm{Im}(\eta) = 0$; (*b*) $\mathrm{Re}(\eta) = -0{\cdot}9506$; (*c*) $\mathrm{Im}(\eta) = -1{\cdot}0625$; (*d*) $\mathrm{Re}(\eta) = 1{\cdot}0494$; (*e*) $\mathrm{Im}(\eta) = 0$. Inviscid solution: ——, real part; - - - -, imaginary part. Viscous solution: – – –, real part; · · · · ·, imaginary part.

η	Inviscid	Viscous
$-0{\cdot}9506$	$(0{\cdot}2904 + 0{\cdot}0115i)$	$(0{\cdot}2910 - 0{\cdot}8 \times 10^{-4}i)$
$(-0{\cdot}9506 - 1{\cdot}0625i)$	$(0{\cdot}1712 - 0{\cdot}3673i)$	$(0{\cdot}1737 - 0{\cdot}3692i)$
$-1{\cdot}0625i$	$(0{\cdot}9865 - 0{\cdot}0008i)$	$(0{\cdot}9763 - 0{\cdot}0071i)$
$(1{\cdot}0494 - 1{\cdot}0625i)$	$(0{\cdot}1480 + 0{\cdot}2977i)$	$(0{\cdot}1516 + 0{\cdot}2926i)$
$1{\cdot}0494$	$(0{\cdot}2867 - 0{\cdot}0221i)$	$(0{\cdot}2889 - 0{\cdot}0259i)$

TABLE 2. Comparison of viscous and inviscid damped eigensolutions.

associated with the axial variation, in amplitude and phase, of the pressure fluctuations. Denoting this pressure fluctuation by $G_+(x)$ and $G_-(x)$ above and below the shear layer respectively it can be seen from equation (4.8) that

$$\frac{1}{G_+}\frac{dG_+}{dx} = i\alpha_+ \quad \text{and} \quad \frac{1}{G_-}\frac{dG_-}{dx} = i\alpha_-. \tag{4.13}$$

These equations may be integrated numerically. The initial conditions for the integration are

$$x_0 = 1/\epsilon, \quad G_+ = 1{\cdot}0, \quad G_- = C_0, \tag{4.14}$$

δ_0^* is taken to be $\delta_\omega^*/\pi^{\frac{1}{2}}$, where δ_ω^* is the vorticity thickness, and the value of C_0 is obtained from the local eigensolution for the initial local frequency. The axial variation of

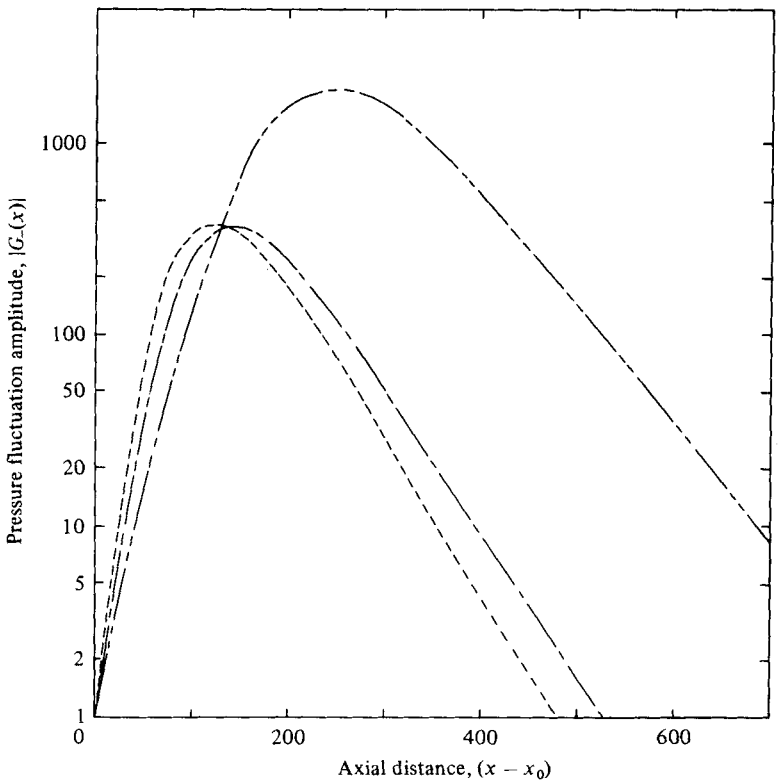

FIGURE 10. Variation of pressure amplitude below shear layer with axial distance, $\omega = 0{\cdot}05$. ····, $M = 0{\cdot}75$; – – –, $M = 1{\cdot}25$; – · – · –, $M = 1{\cdot}75$.

$G_-(x)$ as a function of free-stream Mach number for a fixed real frequency, $\omega = 0{\cdot}05$, is shown in figure 10. As the Mach number increases so the location of the peak amplitude moves further downstream. The location of the peak corresponds to the neutrally stable condition. Although the local frequency for a neutral solution decreases with Mach number, see figure 5, the spread rate of the shear layer decreases with Mach number, the net effect moving the neutrally stable point further downstream. The rate of growth of the fluctuation is more rapid than its decay rate. The initial growth rate is higher for the lower Mach numbers which can also be seen in figure 5. The axial variation in $G_-(x)$ as a function of frequency for a fixed Mach number of 1·75 is shown in figure 11. As the frequency decreases so the location of the amplitude peak moves downstream. The peak amplitude also increases as the frequency decreases. These effects are a result of the similarity of the basic flow profile. The cycle of growth and decay of the pressure fluctuations plays a crucial role in the noise-radiation mechanism. The amount of energy that radiates noise depends on the amplitude of the axial wavenumber component spectrum associated with the pressure fluctuations. In this paper far-field noise radiation calculations will only be presented for radiation into the stationary medium, namely, below the layer. The wavenumber component spectrum for $G_-(x)$ given by

$$\bar{g}_{0_-}(k) = \frac{1}{2\pi}\int_{-\infty}^{\infty} G_-(x)\, e^{-ikx}\, dx \tag{4.15}$$

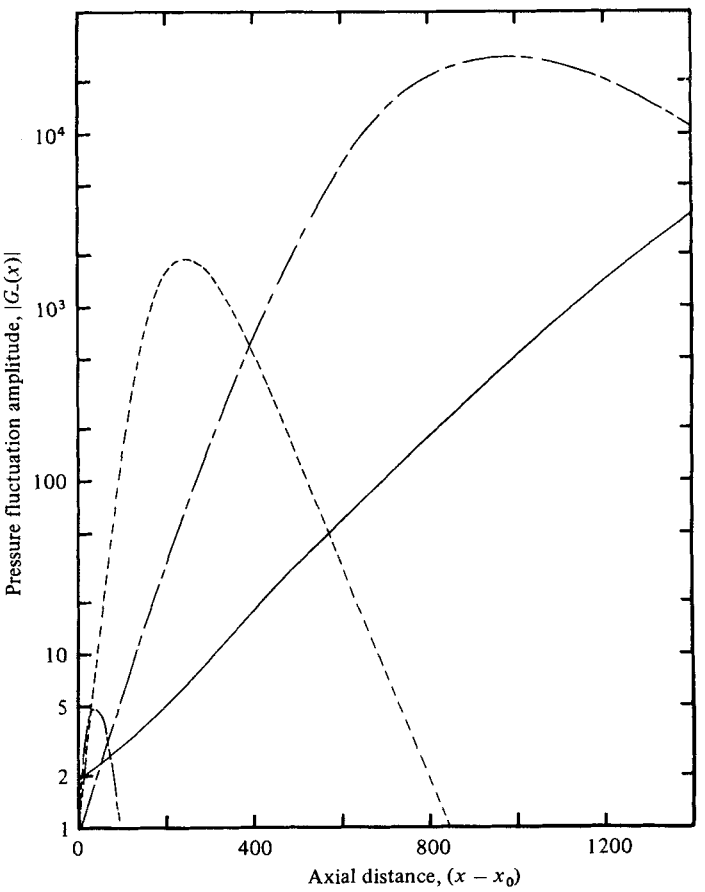

FIGURE 11. Variation of pressure amplitude below shear layer with axial distance, $M = 1{\cdot}75$. ——, $\omega = 0{\cdot}005$; – – –, $\omega = 0{\cdot}015$; - - - - -, $\omega = 0{\cdot}05$; – – –, $\omega = 0{\cdot}15$.

was calculated numerically using the FFT algorithm described by Brigham & Morrow (1967). The amplitude and phase of $\bar{g}_{0-}(k)$, for $\omega = 0{\cdot}05$ and $M = 1{\cdot}75$ are shown in figure 12. The spectrum was found to be insensitive to the number of points used in the transform and the method of truncating the value of $G_-(x)$ for $x < x_0$ and large values of x. This spectrum exhibits features which are characteristic of all the calculated spectra. The dominant peak in the spectrum occurs at a wavenumber which gives a corresponding phase velocity of approximately one half the free-stream velocity.

The directivity patterns of radiated noise are readily obtained using equation (3.26). The directivity patterns for several frequencies are shown in Figure 13 for $M = 1{\cdot}75$. The levels are arbitrarily normalized with respect to the peak level for $\omega = 0{\cdot}005$. The noise radiation peaks at 20 degrees to the axis of the shear layer in the ambient medium. The radiation patterns for all frequencies are similar. This reflects the basic similarity of the shear layer itself where, except at the highest frequencies which will be strongly influenced by the initial shear layer thickness, the development of each frequency wave is similar. As the frequency decreases so the relative sound pressure level in the far field increases. Since the shear layer is infinite in the downstream

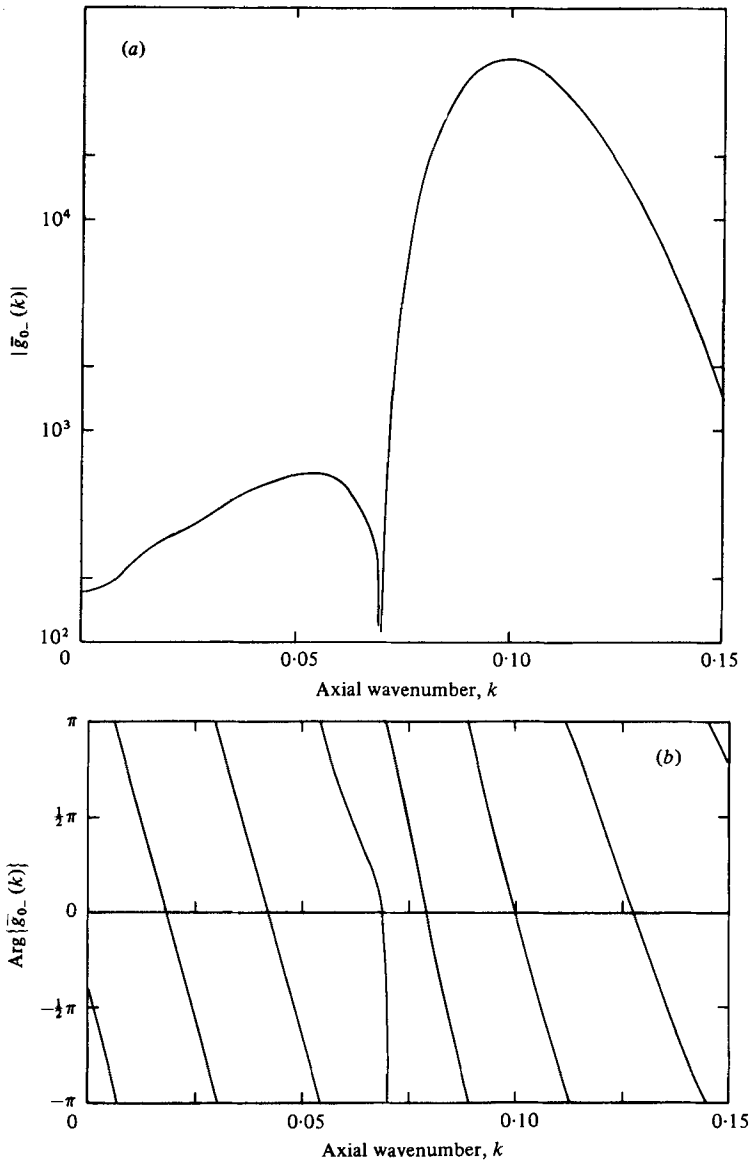

FIGURE 12. Wavenumber component spectrum, $\bar{g}_{0-}(k)$, $\omega = 0{\cdot}05$, $M = 1{\cdot}75$. (*a*) Amplitude; (*b*) phase.

direction the lower the frequency of the wave the greater will be its peak amplitude in the near and far fields. For an experimentally generated shear layer or the mixing region of an axisymmetric jet there will be some non-extreme frequency which will give the greatest amount of radiated noise.

The radiated noise as a function of Mach number is shown in figure 14 for a frequency of $\omega = 0{\cdot}005$. The normalization is the same as in figure 13. For the $M = 1{\cdot}25$ case the noise radiation peaks at 12 degrees to the shear layer axis, while there is no discernible peak for the $M = 0{\cdot}75$ case. The ripples that occur for the two lowest Mach numbers reflect the limitations of the accuracy of the description of $G_{-}(x)$ and its

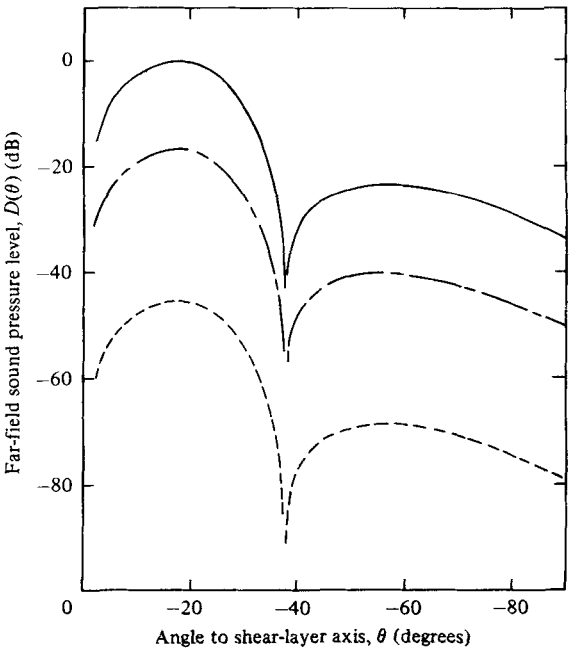

FIGURE 13. Far-field noise directivity patterns, $M = 1{\cdot}75$.
——, $\omega = 0{\cdot}005$; – – –, $\omega = 0{\cdot}015$, - - - - -, $\omega = 0{\cdot}05$.

Fourier transform and are discussed below. The noise radiation from the large-scale structure with its characteristic peak close to the downstream axis is seen to become increasingly efficient as the Mach number increases. As can be seen from equation (3.26), the directivity pattern in the far field is governed by the wavenumber component spectrum amplitude as a function of wavenumber and a $\sin^2\theta$ weighting factor. For Mach numbers such that the peak energy wavenumbers do not radiate noise, that is for $M < 2$, the location of the peak radiation angle is dominated by the $\sin^2\theta$ weighting factor. For higher Mach numbers, the peak will depend more on the peak amplitude wavenumber of the wavenumber component spectrum, i.e. $\theta_{\text{peak}} \simeq \cos^{-1}(2/M)$: $M > 2$, though the $\sin^2\theta$ factor will prevent the peak angle from occurring at less than 20 degrees.

Returning to the ripples on the directivity patterns for $M = 1{\cdot}25$ and $0{\cdot}75$ in figure 14, it should be recalled that only those wavenumber components of the pressure fluctuation at the edge of the flow field which have a sonic phase velocity to some location in the far field can radiate noise. The lower the free-stream Mach number, the smaller is the wavenumber bandwidth that can radiate noise and the further these wavenumbers will be from the peak amplitude number. The amplitude of the wavenumber component spectra for $\omega = 0{\cdot}05$ and various Mach numbers is shown in figure 15. The arrows indicate the range of wavenumber components that contribute to the noise radiation. For the higher Mach number, a significant portion of the energy is radiated. However, the region that radiates noise in the subsonic case is far from the peak amplitude wavenumber. The amplitude of components that do radiate at $M = 0{\cdot}75$ are a factor of 10^3 below the peak level at that frequency and are thus very sensitive to the exact description of the pressure fluctuations in the near field. Thus,

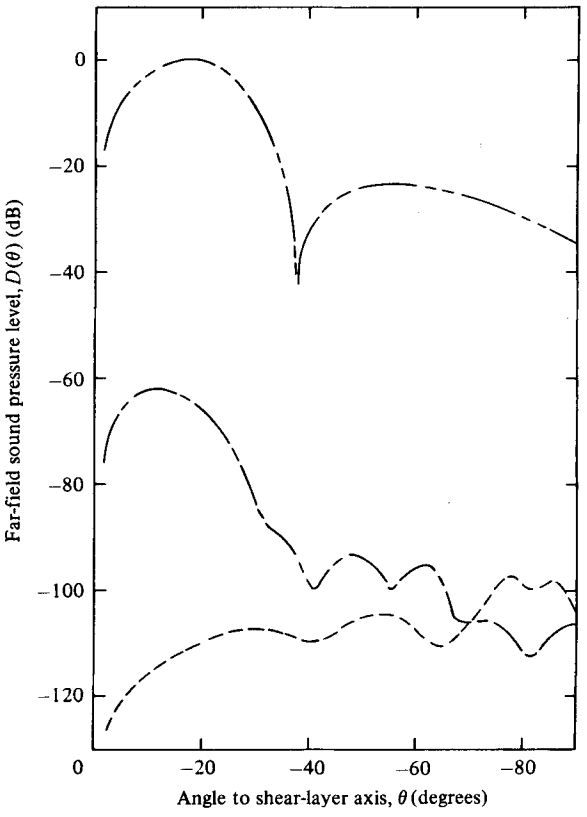

FIGURE 14. Far field noise directivity patterns, $\omega = 0{\cdot}005$.
$-\cdot\cdot-$, $M = 1{\cdot}75$; $-\cdot-$, $M = 1{\cdot}25$; $\cdot\cdot\cdot\cdot\cdot$, $M = 0{\cdot}75$.

though a mechanism by which the large-scale fluctuations in the subsonic shear layer radiate noise has been demonstrated, the calculated radiated noise level should be regarded with caution. The calculated directivity patterns for the supersonic shear layers, however, do have quantitative significance.

5. Concluding remarks

In this paper it has been demonstrated how the multiple-scales asymptotic expansion for an instability wave in a turbulent shear layer may be continued to large distances from the shear layer. The extended solution has been used to calculate the noise radiation associated with the instability wave. The same technique may, of course, be applied to other configurations such as jets, wakes, boundary layers, etc. The multiple-scales expansion was used to take account of the small divergence effect of the mean flow. Although locally this effect is small, from a global point of view, it is extremely important. First of all, it is this growth of the mean flow that causes any initially unstable wave to be ultimately damped out far downstream. This effectively removes the problem of unstable waves attaining unbounded amplitudes as the parallel flow approximation would imply. Secondly, as a result of this spatial growth and decay of the wave amplitude, the wavenumber spectrum of a discrete frequency wave is

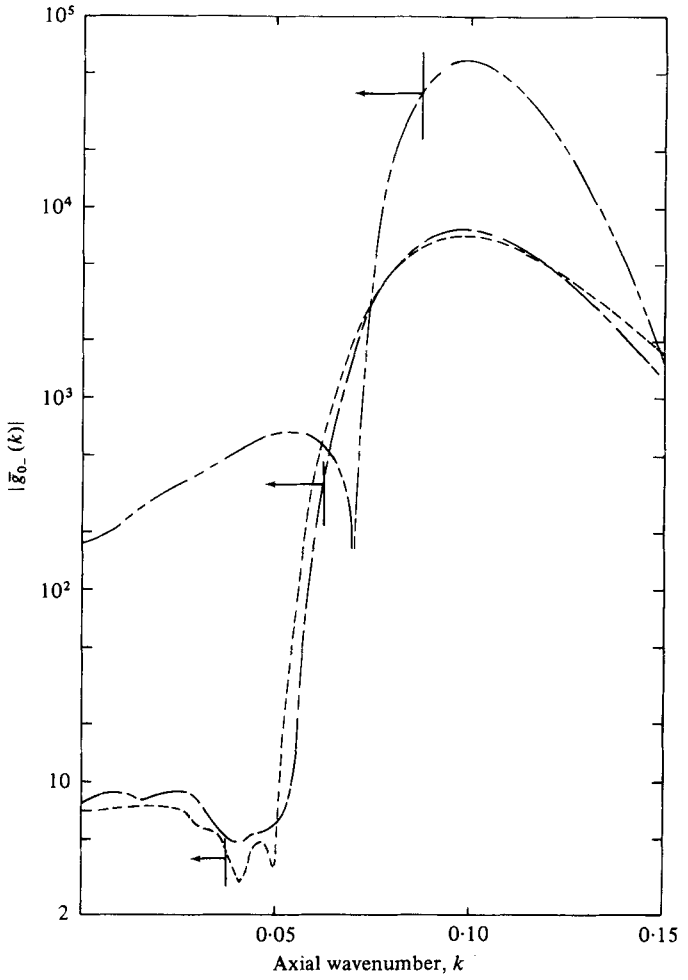

FIGURE 15. Amplitude of wavenumber component spectrum, $|\bar{g}_{0-}(k)|$, $\omega = 0{\cdot}05$. ——·——, $M = 1{\cdot}75$; – – –, $M = 1{\cdot}25$; · · · · ·, $M = 0{\cdot}75$.

broadband instead of discrete. Since only the part of the broadband wave spectrum with supersonic phase velocities could lead to radiation of sound, this feature is crucial to the problem under consideration.

In § 4, the numerical results suggest that noise generated by instability waves could be very important for supersonic flow and that noise is predominantly radiated to angles quite close to the direction of flow. This is in agreement with the experimental observations of McLaughlin *et al.* (1977) and Dosanjh & Yu (1968). However, it is necessary to point out here that the present two-dimensional shear-layer model does not simulate fully an axisymmetric jet flow. In a real jet, the mean flow consists of three distinct regions. Close to the jet exit the flow comprises a uniform core surrounded by a mixing layer. At about four to five diameters downstream of the nozzle exit for subsonic jets and further downstream for supersonic jets, the mixing layers merge to form a short transition region. In this region, the flow undergoes certain adjustments and develops still further downstream into a self-similar flow generally referred to as

the fully-developed region. Owing to these changes in mean flow characteristics, it is expected that the corresponding wave spectrum would be much broader and with more supersonic phase velocity components. This, in turn, suggests that the instability-wave noise-generation mechanism is probably more effective in jets than in plane shear layers. Therefore, the present numerical results, especially those on subsonic flows, should not be used to draw firm conclusions with regard to noise associated with jets. Some preliminary calculations have been made by the authors for the noise radiation by instability waves in supersonic jets, using the technique described in this paper. The results show close agreement between measured and calculated near- and far-field sound pressure levels.

The work of one of the authors (C.K.W.T.) was supported by N.A.S.A. Langley Research Center, under Grant NSG 1329; the other author (P.J.M.) acknowledges the support of the Air Force Aero Propulsion Laboratory, under Contract F33615-76-C-2021.

Appendix A

The coefficients, B_i, in (2.21) are given by:

$$B_1 = -2i\beta[M^2U\hat{\beta}+k_0]; \tag{A 1}$$

$$B_2 = \frac{2i\beta^2}{\hat{\beta}^2}\frac{dU}{d\eta}; \tag{A 2}$$

$$B_3 = i(M^2U^2-1)\beta; \tag{A 3}$$

$$B_4 = \frac{2iU\beta^2}{\hat{\beta}^3}\frac{dU}{d\eta}; \tag{A 4}$$

$$B_5 = i\left\{k_0(1-M^2U^2)+k_0M^2\left[U\frac{dV}{d\eta}-V\frac{dU}{d\eta}\right]+\frac{2k_0^3V}{\hat{\beta}^2}\frac{dU}{d\eta}-\frac{2k_0^2(k_0U-\hat{\beta})}{\hat{\beta}^2}\frac{dV}{d\eta}\right\}; \tag{A 5}$$

$$B_6 = i\left\{\frac{2k_0^2U}{\hat{\beta}^3}\frac{dU}{d\eta}\frac{dV}{d\eta}+2\eta[k_0+M^2U\hat{\beta}]-2M^2V\hat{\beta}-\frac{2k_0^3V}{\hat{\beta}^3}\left(\frac{dU}{d\eta}\right)^2-\frac{2\beta^2}{\hat{\beta}^3}\frac{dU}{d\eta}\right\}. \tag{A 6}$$

The functions h_1 and h_2 in (2.23) are given by

$$h_1 = 2\left\{k_0\xi+M^2U\hat{\beta}\xi-\frac{\beta}{\hat{\beta}^2}\frac{dU}{d\eta}\frac{\partial\xi}{\partial\eta}\right\} \tag{A 7}$$

and

$$h_2 = 2\left\{\frac{k_0}{\hat{\beta}^2}\frac{dU}{d\eta}\frac{\partial\xi}{\partial\eta}-2M^2\hat{\beta}\xi\right\}. \tag{A 8}$$

Appendix B. Inviscid damped-wave solution and integration contour

The purpose of this appendix is to clarify two outstanding questions concerning damped-wave solutions of an inviscid fluid as used in § 2. Firstly, it has been pointed out (Lin 1955, ch. 8) that the limiting damped-wave solution of the Orr–Sommerfeld equation does not satisfy the inviscid Orr–Sommerfeld equation over the entire

interval of the real axis which corresponds to the physical domain of the problem. Thus extreme care must be exercised in selecting the mathematically- and physically-correct solution of the inviscid model. Secondly, the integrals of (2.20) and (2.21) which arise because of the imposition of a solvability condition on the slightly non-parallel flow solution can no longer be carried out along the real y axis as the eigenfunction ξ is not completely defined there. In the past, the first question has been resolved by appealing to the effect of viscosity as discussed by Lin (1955) and implemented numerically by Mack (1965). Here two slightly different ways of dealing with both questions without invoking viscous effects will be presented. It is believed that these analytical approaches, in addition to serving as a complement to the numerical verification study of the inviscid damped-wave solution discussed in § 4.2, can actually offer some insight into the physics of the problem.

B 1 *Wave propagation approach*

This approach is an extension of that given in the appendix of Tam (1975). Here the basic idea is to follow the actual propagation of a hydrodynamic wave from the initial region of the mixing layer where it is unstable to the downstream region where, because of the increase in mixing-layer thickness, it becomes damped. It is well known that the inviscid Orr–Sommerfeld problem, equations (2.13) and (2.14), gives mathematically- and physically-correct unstable solutions (of course only as a large-Reynolds-number approximation). Thus the correct inviscid damped wave solution can be found as the analytic extension of the unstable solution as the mixing-layer thickness parameter s increases. Equation (2.13) is a second-order differential equation with a regular singular point at $\eta_c(s)$ where $\hat{\beta} = \beta(s) - k_0 U(\eta_c) = 0$. This point has been referred to as a critical point by Lin (1955) in considering the full fourth order Orr–Sommerfeld equation. A simple Frobenius series analysis (Boyce & DiPrima 1977, ch. 4) shows that the indicial equation has two roots which differ by an integer so that the general solution has a logarithmic singularity at $\eta_c(s)$. For the mean flow profile given by equation (4.1) the critical point $\eta_c(s)$ lies above the real η axis for an unstable wave as shown in figure 16(*a*). Since the inviscid unstable solution is valid for all values of η along the real axis, the branch cut of the logarithmic function of the solution must extend from η_c to infinity in the upper-half η plane. Without loss of generality one can choose the branch cut to be parallel to the imaginary η axis as shown in figure 16(*a*). Now as the unstable wave propagates downstream the parameter s increases so that $\eta_c(s)$ moves toward the real η axis and eventually crosses it into the lower half-plane when the wave becomes damped. Now to preserve analyticity of solution, i.e. the inviscid damped-wave solution must be the analytic continuation of the inviscid unstable wave solution, the contour of integration must be deformed so as to remain below the branch cut as shown in figure 16(*b*). This contour deformation applies to the integration path for the eigenfunction ξ as well as to the integrals of (2.20) and (2.21). For an inviscid damped wave the value of the eigenfunction on the two sides of the branch cut along the real axis will not be the same. That is the eigenfunction is discontinuous at the branch cut. It has been pointed out by Tam (1975) that physically for an inviscid fluid the branch cut represents a critical layer of infinitesimal thickness. The discontinuity across this layer would be smoothed out if viscosity or other diffusive mechanisms were taken into account. In that case the thickness of the critical layer would be finite.

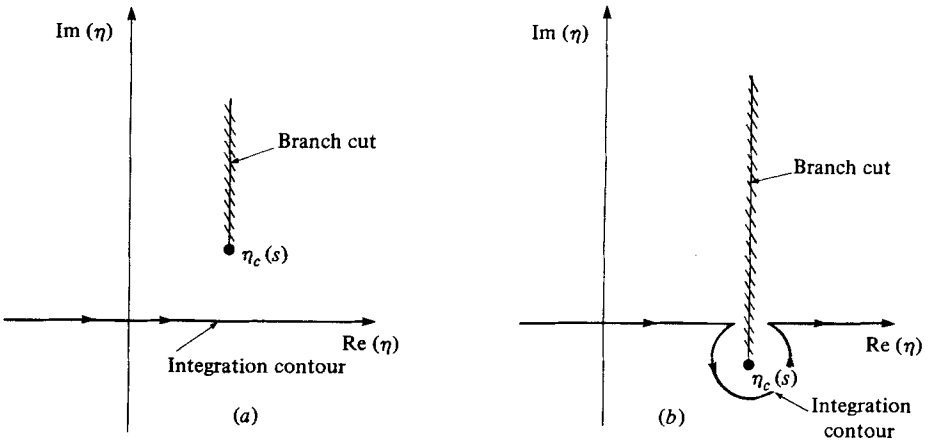

FIGURE 16. Critical or branch point, integration contour and branch cut in the complex η plane. (*a*) Inviscid unstable wave; (*b*) inviscid damped wave as analytic continuation of inviscid unstable wave when s increases.

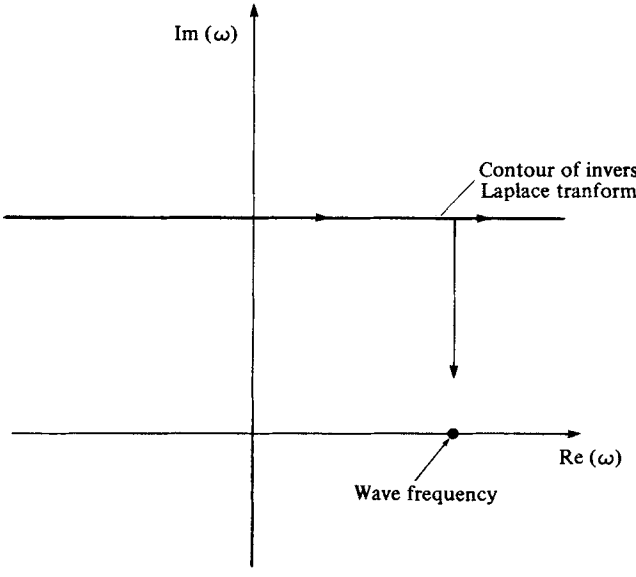

FIGURE 17. Complex ω plane showing the initial position of the contour of inverse Laplace transform.

B 2 *Initial-value approach*

An alternative way is to consider the inviscid Orr–Sommerfeld problem as an initial boundary-value problem (see Dikii 1960; Tam 1971, 1978). In this case by applying a Laplace transform to t the mathematical problem reduces formally to the same one as before, namely, consisting of (2.12) and (2.14). The only difference is that $\omega(\beta = \omega s)$ is now the complex-Laplace-transform variable. To satisfy the causality condition the relative positions of all the contours of integration and singularities are to be determined by first setting the inverse Laplace transform contour above all poles and singularities of the integrands in the complex ω plane as shown in figure 17.

Since ω in (2.13) and (2.14) represents a value of ω on this inverse transform contour, the relative positions of the branch cut of the logarithmic function of the solution and integration contours for ξ and equations (2.20) and (2.21) are, therefore, to be decided with Im (ω) set equal to a large positive value initially. For the problem at hand it is straightforward to find that the branch or critical point η_c lies above the real η axis and hence it is also above the contours of integration. Now to obtain a solution with ω equal to a positive real value, the inverse transform contour can be deformed to the real ω axis. When this process of contour deformation is being carried out the branch point in the complex η plane moves towards the real axis. For an inviscid damped wave η_c would actually move below the real axis so that to preserve analyticity all the contours of integration in the η plane which originally were along the real axis must now be deformed below this point as shown in figure 16(b). In so doing the solution obtained by the wave propagation approach above is, once again, recovered.

It is to be noted that the above discussion is based on the implicit assumption that the inviscid fluid model can, if the appropriate discontinuity is inserted when necessary, give a reasonably good, physically realizable, overall description of the instability-wave problem. This is reminiscent of the use of weak solutions (with shocks and discontinuities) in supersonic gasdynamics and the analytic continuation solution in plasma kinetic theory involving Landau damping. However, it has not been proved (but has been demonstrated numerically in §4.2) that the damped inviscid solution is the limit of the solution of the Orr–Sommerfeld equation as the Reynolds number tends to infinity. Such a proof, although essential for mathematical rigour, is beyond the scope of this paper.

REFERENCES

Betchov, R. & Criminale, W. O. 1967 *Stability of Parallel Flows*. Academic.

Bishop, K. A., Ffowcs Williams, J. E. & Smith, W. 1971 On the noise sources of the unsuppressed high speed jet. *J. Fluid Mech.* **50**, 21–31.

Blumen, W. 1970 Shear layer instability of an inviscid compressible fluid. *J. Fluid Mech.* **40**, 769–781.

Blumen, W. 1971 Jet flow instability of an inviscid compressible fluid. *J. Fluid Mech.* **46**, 737–747.

Bouthier, M. 1972 Stabilité linéaire des écoulements presque parallèles. Partie I. *J. Méc.* **11**, 599–621.

Bouthier, M. 1973 Stabilité linéaire des écoulements presque parallèles. Partie II. La Couche Limite de Blasius. *J. Méc.* **12**, 75–95.

Boyce, W. E. & DiPrima, R. C. 1977 *Elementary Differential Equations*, 3rd edn. Wiley.

Brigham, E. O. & Morrow, R. E. 1967 The fast Fourier transform. *I.E.E.E. Spectrum*, *December*, pp. 63–70.

Chan, Y. Y. 1974*a* Spatial waves in turbulent jets. *Phys. Fluids* **17**, 46–53.

Chan, Y. Y. 1974*b* Spatial waves in turbulent jets. Part II. *Phys. Fluids* **17**, 1667–1670.

Chan, Y. Y. 1975 Nonlinear spatial wave development in an axisymmetric turbulent jet. *Nat. Res. Counc., Canada, Nat. Aero. Est. Aero. Rep.* LR-585.

Chan, Y. Y. 1976 Spatial waves of higher order modes in an axisymmetric turbulent jet. *Phys. Fluids* **19**, 2042–2043.

Crighton, D. B. & Gaster, M. 1976 Stability of slowly diverging jet flow. *J. Fluid Mech.* **77**, 397–413.

Dahan, C. & Élias, G. 1976 Source structure pattern in a hot jet by infrared-microphones correlations. *A.I.A.A. Paper* 76-542.

DIKII, L. A. 1960 The stability of plane parallel flows of an ideal fluid. *Sov. Phys. Dokl.* **135**, 1179–1182.

DOSANJH, D. S. & YU, J. C. 1968 Noise from underexpanded axisymmetric jet flow using radial jet flow impingement. *Proc. AFOSR-UTIAS Symp. Aerodyn. Noise, Toronto, Canada.*

GASTER, M. 1974 On the effects of boundary-layer growth on flow stability. *J. Fluid Mech.* **66**, 465–480.

GROPENGIESER, H. 1969 Bietrag zur Stabilität freier Grenzschichten in kompressiblen Medien. *Deutsch Luft-und Raumfahrt* FB 69-25, Berlin.

LAU, J. C., MORRIS, P. J. & FISHER, M. J. 1976 Turbulence measurements in subsonic and supersonic jets using a laser velocimeter. *A.I.A.A. Paper* no. 76, 348.

LEES, L. & LIN, C. C. 1946 Investigation of the stability of the laminar boundary layer in a compressible fluid. *N.A.C.A. Tech. note* 1115.

LIEPMANN, H. W. & LAUFER, J. 1947 Investigations of free turbulent mixing. *N.A.C.A. Tech. Note* 1257.

LIN, C. C. 1953 On the stability of laminar mixing region between two parallel streams in a gas. *N.A.C.A. Tech. Note* 2887.

LIN, C. C. 1955 *The Theory of Hydrodynamic Stability*. Cambridge University Press.

LIU, J. T. C. 1974 Developing large-scale wave-like eddies and the near-jet noise field. *J. Fluid Mech.* **62**, 437–464.

MACK, L. M. 1965 Computation of the stability of the laminar compressible boundary layer. *Methods in Comp. Phys.* **4**, 147–299.

MCLAUGHLIN, D. K., MORRISON, G. L. & TROUTT, T. R. 1975 Experiments on the instability waves in a supersonic jet and their acoustic radiation. *J. Fluid Mech.* **69**, 73–95.

MCLAUGHLIN, D. K., MORRISON, G. L. & TROUTT, T. R. 1977 Reynolds number dependence in supersonic jet noise. *A.I.A.A. J.* **15**, 526–532.

MERKINE, L. & LIU, J. T. C. 1975 On the development of noise-producing large-scale wave-like eddies in a plane turbulent jet. *J. Fluid Mech.* **70**, 353–368.

MICHALKE, A. 1971 Instabilität eines kompressiblen runden Freistrahls unter Berücksichtigung des Einflusses der Strahlgrenzschichtdicke. *Z. Flugwiss.* **19**, 319–328.

MOORE, C. J. 1977 The role of shear layer instability waves in jet exhaust noise. *J. Fluid Mech.* **80**, 321–367.

MORRIS, P. J. 1974 A model for the structure of jet turbulence as a source of noise. *A.I.A.A. Paper* 74, 1.

MORRIS, P. J. 1976*a* The flow and acoustic characteristics of the large-scale wave-like structure of an axisymmetric jet. In *The Generation and Radiation of Supersonic Jet Noise* (ed. H. E. Plumblee), vol. 2, ch. 4 (AFAPL-TR-76-65).

MORRIS, P. J. 1976*b* The spatial viscous instability of axisymmetric jets. *J. Fluid Mech.* **77**, 511–529.

MORRIS, P. J. 1977 Flow characteristics of the large-scale wave-like structure of a supersonic round jet. *J. Sound Vib.* **53**, 223–244.

PATEL, R. P. 1973 An experimental study of a plane mixing layer. *A.I.A.A. J.* **11**, 67–71.

SARIC, W. S. & NAYFEH, A. H. 1975 Nonparallel stability of boundary layer flows. *Phys. Fluids* **18**, 945–950.

SEDEL'NIKOV, T. K. 1967 The frequency spectrum of the noise of a supersonic jet. *Phys. Aero. Noise Moscow: Nauka.* (Trans. 1969 *NASA* TTF-538, pp. 71–75.)

TAM, C. K. W. 1971 Directional acoustic radiation from a supersonic jet generated by shear layer instability. *J. Fluid Mech.* **46**, 757–768.

TAM, C. K. W. 1972 On the noise of a nearly ideally expanded supersonic jet. *J. Fluid Mech.* **51**, 69–95.

TAM, C. K. W. 1975 Supersonic jet noise generated by large-scale disturbances. *J. Sound Vib.* **38**, 51–79.

TAM, C. K. W. 1978 Excitation of instability waves in a two-dimensional shear layer by sound. *J. Fluid Mech.* **89**, 357–371.

VAN DYKE, M. 1975 *Perturbation Methods in Fluid Mechanics*. Stanford, California: Parabolic.